# Evaluating the Role of Atmospheric Stability in Generating Asymmetrical Precipitation During the Landfall of Hurricane Florence (2018)

Lindsey Morrison

Thesis submitted to the faculty of the Virginia Polytechnic Institute and State University in partial fulfillment of the requirements for the degree of

Master of Science
In
Geography

Stephanie Zick, Chair
Andrew Ellis
Craig Ramseyer

December 11, 2020
Blacksburg, Virginia

Keywords: tropical cyclone, hurricane, precipitation, convection, atmospheric stability

**Evaluating the Role of Atmospheric Stability in Generating Asymmetrical Precipitation During the Landfall of Hurricane Florence (2018)**

Lindsey Morrison

## ABSTRACT

Hurricane Florence (2018) was unique due to its slow storm motion during landfall, causing convective rainbands to produce high amounts of precipitation along the coast of North Carolina. This study focuses on the relationship between precipitation asymmetries and atmospheric stability surrounding the tropical cyclone (TC) during the landfall period of a nearly-stationary TC. Previous research with idealized hurricane simulations suggests that atmospheric stability may vary surrounding a TC during landfall, with the atmosphere destabilizing offshore and stabilizing onshore. However, this finding has not been studied using a realistic approach. Due to Hurricane Florence's slow motion, the storm was situated at the land-ocean boundary for multiple days, providing an ideal opportunity to examine the role of atmospheric stability in modifying hurricane precipitation during landfall. This study uses the Advanced Research Weather Research and Forecasting (WRF-ARW) version 3.6.1 to produce high-resolution simulations to examine the variations in precipitation and atmospheric stability surrounding Hurricane Florence. Precipitation accumulation at different temporal scales was used to determine that asymmetries existed during the landfall period. Observed and model-simulated Convective Available Potential Energy (CAPE) were used to measure stability surrounding the TC. Simulated CAPE indicates that there was a significant difference between stability right- and left-of-track. In addition to a control simulation, two experimental simulations were conducted by modifying the land surface to vary the heat and moisture exchange coefficient (HS) and hold the surface roughness ($Z_0$) constant. By isolating the HS to be more moist or dry, the altered low-level moisture was hypothesized to cause the precipitation and convection distributions to become more symmetrical or asymmetrical, respectively. The results from the experimental simulations showed that the altered land surface affects the relative humidity from the surface to 950 mb, which has an immediate impact on stability off-shore left-of-track. Overall, the precipitation and stability asymmetries were not significantly impacted by the altered near-surface moisture, indicating other physical factors contribute to the asymmetries. The results of this study provide insight into the role of atmospheric instability in generating asymmetrical precipitation distributions in landfalling TCs, which may be particularly important in slow-moving TCs like Hurricane Florence.

**Evaluating the Role of Atmospheric Stability in Generating Asymmetrical Precipitation During the Landfall of Hurricane Florence (2018)**

Lindsey Morrison

GENERAL AUDIENCE ABSTRACT

Landfalling tropical weather systems such as hurricanes can significantly impact coastal communities due to severe flooding and damaging winds. Hurricane Florence (2018) affected coastal and inland communities in North Carolina and South Carolina when the storm produced a significant amount of precipitation over the coastal region. During landfall, the center of Hurricane Florence moved slowly parallel to the coastline, which creates a suitable time frame to isolate and study the influence of landfall on precipitation asymmetries. Precipitation asymmetry occurs when more rainfall falls on one side of the hurricane; for example, heavier precipitation tends to occur on the right side of a hurricane during the landfall period. Hurricane rainbands that are responsible for producing heavy precipitation form in areas where there is higher moisture near the surface while lighter precipitation forms in areas where there is drier air near the surface. This study focuses on the relationship between land surface moisture and spatial variations of precipitation during the hurricane landfall period by studying observations and model simulations of Hurricane Florence. The model simulation of Hurricane Florence found that more precipitation fell on the right side of the storm, indicating that there was precipitation asymmetry. In order to understand how the precipitation asymmetries form, the model simulation of Hurricane Florence was modified to create two experiments. In the first experiment, the land surface was altered to have a moister land surface, which should cause the hurricane precipitation to be more symmetrical. In the second experiment, the land surface was altered to have a drier land surface, which should cause stronger precipitation asymmetry. However, the results did not match this expectation. Instead, both experiments simulated asymmetrical precipitation with more precipitation falling on the right side of each storm during the landfall period. These results suggest that the modified land surface moisture did not have a significant impact on the formation of precipitation asymmetries. Other factors are therefore suggested to have a more dominant influence on the development of precipitation. Overall, this work can support future studies by ruling out the impact of land surface moisture on a hurricane's precipitation formation during the landfall period.

ACKNOWLEDGEMENTS

I would like to extend my sincere gratitude to the many individuals who have continuously supported my academic achievements and personal successes during my time in graduate school.

I am especially grateful for the guidance from my advisor, Stephanie Zick. Her continuous mentorship and positive demeanor encouraged me to keep my composure and continue to achieve my academic and personal goals. I could not have asked for a better mentor.

Additionally, I want to thank my committee members, Dr. Andrew Ellis and Dr. Craig Ramseyer, who provided different perspectives and useful feedback for this research. I also want to send my thanks to the Department of Geography for providing me the opportunity to be a contributing member of the department. Many thanks also go out to my friends, near and far, for always keeping me in good spirits. The page count would dramatically increase if I listed every person, but if you're taking the time to read this, I imagine your name would make the list.

Finally, I want to thank my fiancé, Shawn, who has continued to support my aspirations in life. Thank you for all the adventures that helped take my mind off coding and writing.

If you have made it this far and are ready to read, I have one request… Sit back, grab your favorite beverage, and enjoy reading the next 66 pages of this paper!

## Table of Contents

## Chapter 1: Introduction

Communities located along the Atlantic coastline in the United States (U.S.) are in a prime location to be impacted by tropical cyclones (TCs). TCs are a tropical-originating meteorological phenomenon that produce damaging winds, extreme rainfall, and impactful storm surge. While TCs form over open water, they can also move onto land, a process known as landfall. Landfalling TCs can significantly impact coastal communities due to the production of damaging winds and flooding. As the population increases along the U.S. Gulf and East Coasts, vulnerability to economic loss and infrastructural damage increases dramatically (Klotzbach et al., 2018). The focal point of this study is Hurricane Florence (2018), a TC that made landfall in the southeastern United States in 2018 and produced extreme rainfall.

Hurricane Florence impacted much of the southeastern U.S., with the most notable effects in North Carolina and South Carolina. Hurricane Florence was a unique storm due to slower storm motion at the time of landfall. Due to the slow storm motion, the rainbands that moved over land continuously tracked over the same area of North Carolina; this caused approximately 762 mm (30 in) of rainfall to occur in that area (Stewart & Berg, 2019). Widespread inland flooding, induced by the high amount of precipitation, was the cause of 11 direct deaths in North Carolina and four deaths in South Carolina (Stewart & Berg, 2019). The National Oceanic and Atmospheric Administration (NOAA) National Centers for Environmental Information (NCEI) estimates that Hurricane Florence caused approximately $24 billion in wind and water damage in the United States (Stewart & Berg, 2019). Many homeowners were significantly impacted by flood damage and lack of flood insurance, which caused an increase in the economic impact (Paul et al., 2019). Inland flooding in North Carolina caused severe

environmental impacts due to the discharge of contaminants into waterways from several livestock and coal plant locations (Paul et al., 2019).

The evolution of the rainbands during landfall is of primary interest in this study. Earlier work on TC landfall used idealized models to investigate the influence of environmental variables on the structure and spatial patterns of TC precipitation around and during landfall (Johnny C.L. Chan & Liang, 2003). Another previous idealized study investigated the different thermodynamic characteristics between the rainbands in the inner and outer cores (Li & Wang, 2012). Hurricane Florence was not the first TC to slow down during landfall and produce extreme precipitation. For example, Hurricane Harvey (2017) stalled near landfall and produced rainfall totals that were greater than 762 mm (30 in) in most of the greater Houston, Texas area, with local amounts nearing 1524 mm (60 in) (Blake & Zelinsky, 2017). However, a thorough literature review found no studies that simulate TCs to examine the influence of atmospheric stability on the generation of convection in the distant rainbands during landfall. Distant rainbands are often robust, convective features that form in the outer region of the TC, which extends approximately 150-500 km radially away from the TC center (Weatherford & Gray, 1988b). A case study of Hurricane Florence will provide a realistic environment that is appropriate for exploring how convective rainbands interact with the land and atmosphere during landfall. Another objective of this study is to investigate changes in the precipitation distribution of the training rainbands due to the TCs interaction with land and surrounding atmospheric environment. The results of this study will help forecasters improve precipitation forecasting techniques, especially for TCs that have a slower forward speed.

This study will simulate Hurricane Florence around the time of landfall to analyze the effect of landfall on the convection and moisture in the distant rainbands. The influence of land-

ocean interactions on TC asymmetries can be examined during the period of time the TC becomes stationary near the coastline. The impact of the low-level moisture on precipitation and stability surrounding a TC is not well-known. Chan and Liang 2003 proposed that the horizontal and vertical distributions of moist and dry air influence the spatial distribution of convection surrounding a TC. The layering of a moist boundary layer and drier air aloft can occur when a TC is situated on the land-ocean boundary, allowing the circulation to move stable air masses over the ocean surface. As the air mass moves from left-of-track to right-of-track over the ocean surface, the boundary layer may begin to moisten while dry air persists aloft. This can cause the air mass to destabilize and produce convective precipitation that eventually moves on-shore right-of-track. As the TC circulation continues to advect the air mass over the land surface from right-of-track to left-of-track, the layering of the air mass may form a drier boundary layer with moist air aloft. Drier air near the surface with moist air aloft can cause an air mass to stabilize which favors lighter precipitation to form left-of-track. The TC circulation may continue to transport the stable air mass off-shore left-of-track, allowing destabilization to continue to occur over the ocean surface. Chan and Liang's (2003) theorized stabilizing-destabilizing effect may persist until the TC circulation moves farther inland at which point the asymmetries become primarily caused by other influences, such as topography. An understanding of the convective distribution of the distant rainbands, and how they interact with the surrounding atmosphere, will provide insight into how the rainbands evolve during the landfall period of a slow-moving TC. Hurricane Florence is an excellent case for observing Chan and Liang's (2003) theory because the storm stalled along the coastline around the time of landfall. The positioning of the TC along the coast for an extended period is hypothesized to support asymmetries due to land-ocean interaction and limit asymmetries from the common influences of landfall.

This thesis investigates two main hypotheses. First, I hypothesize that an asymmetrical precipitation distribution can be linked to differences in atmospheric stability surrounding the storm. Next, I hypothesize that the landfalling TC will have a more defined asymmetrical precipitation distribution when the land cover parameter is set to a drier land surface, such as wooded tundra. This is because the moist, tropical air on the right of the TC track will stabilize as it moves over the drier land surface which will cause convective cells to weaken as they move inland. On the left side of the TC track, the air moving offshore will destabilize as it moves over the moist ocean surface, which will lead to the production of convective rainbands that continuously train inland on the right side of the TC track and then weaken. I also hypothesize that when the land cover parameter is set to a moister land surface, the precipitation distribution will be more symmetrical. Due to the increased source of moisture at the surface, the TC will be more balanced, similar to a TC over open water. To address these hypotheses, I will answer the following research questions:

1. **How does atmospheric stability vary surrounding Hurricane Florence during landfall, and how does that contribute to the asymmetrical precipitation distribution?**
2. **How does land surface moisture affect the precipitation distribution of Hurricane Florence during landfall?**

These research questions aim to fill a void in the literature related to how certain environmental factors, such as moisture, influence the precipitation distribution and intensity of the outer rainbands in landfalling tropical cyclones. The results of this study will create a deeper understanding of how distant rainbands interact with the land and the environment. In turn, this

should help forecasters develop better forecasts for precipitation associated with the outer rainbands of tropical cyclones.

# Chapter 2: Literature Review

## 2.1 Tropical Cyclone Climatology

Tropical meteorology is a sub-discipline of meteorology that involves the analysis of atmospheric and weather phenomena that originate at lower latitudes. The discipline of meteorology focuses on the physical processes associated with Earth's atmosphere at numerous spatial and temporal scales (Thomas, 2016). One specific example of a weather phenomenon that occurs in tropical regions at the synoptic scale is a TC. A TC is a low pressure cyclone that forms over a tropical body of water and has a closed circulation (Houze Jr., 2010). The study of TCs often involves the analysis of spatiotemporal patterns associated with variables such as atmospheric conditions, precipitation distribution, and orographic effects. This study will focus on isolating the moisture variable associated with specific land cover types to investigate the influence it has on the precipitation distribution and stability within the distant rainband region.

In the Atlantic Ocean basin, strong TCs are referred to as hurricanes, which have sustained winds greater than 33 meters per second (Houze Jr., 2010). Since Hurricane Florence formed in the North Atlantic Ocean, I will use the terms TC and hurricane interchangeably. Regions of genesis are located over tropical oceans because they provide an abundance of energy from latent heat release (Gray, 1968). In the Atlantic Ocean basin, TCs typically develop between 5°N and 20°N (5°S and 20°S), and not farther equatorward due to the Coriolis force being extremely weak closer to the equator (Houze Jr., 2010). Environmental factors that favor tropical cyclogenesis include sea surface temperatures (SST) greater than 26.5°C, low-level vorticity, and weak vertical shear of the horizontal wind field (Gray, 1968). These factors alone will not generate or sustain the deep convection necessary for TC development. A synoptic-scale forcing mechanism that produces and sustains organized deep convection is a necessary

component for tropical cyclogenesis (Bracken & Bosart, 2000). Bracken and Bosart (2000) identified several synoptic-scale patterns that favor ascent and deep convection in the lower latitudes of the Atlantic basin: African easterly waves, upper-level midlatitude troughs, and old frontal boundaries. As a TC forms in the lower latitudes, it is common for the easterly winds to advect the system westward until the westerlies and the flow of the subtropical high cause the storm motion to shift north and/or eastward (Houze Jr., 2010).

## 2.2 Hurricane Structure

### 2.2.1 Circulations

In the most general sense, the structure of a TC is composed of the primary and secondary circulations. The primary circulation is the broad cyclonic circulation of the wind field (Willoughby, 1988). One of the many features that characterize TCs is the presence of a warm core; this occurs when the temperature in the center of the vortex is significantly greater than the surrounding environment (Halverson et al., 2006; Stern & Nolan, 2012). The warming in the center is caused by latent heat release in the eyewall and subsidence in the eye of the TC (Halverson et al., 2006). An idealized numerical study conducted by Stern and Nolan (2012) concluded that the strongest maximum perturbation temperature is often located from 4 to 7 km in height. The secondary circulation, the in-up-and-out movement of air, is the process that transports energy through the TC and keeps the primary circulation in gradient-wind balance (Willoughby, 1990; Bui et al., 2009).

### 2.2.2 Inner Core and Outer Core

To better understand its structure, a TC may be split into two regions: inner core and outer core (Figure 2.1). The inner core extends from the inner-most region of the vortex to

approximately the point where the outer environment begins to interact more with the system (Shea & Gray, 1973). As depicted in Figure 2.1, the inner core region is commonly characterized by the eye, convective eyewall, principal rainband, and secondary rainband (Houze Jr., 2010). The outer core region of a TC extends from the outer edge of the inner core to the periphery of the vortex and contains the distant rainbands. Some studies using balance dynamics have found that diabatic heating in the secondary circulation influences the spin-up and spatial extent of the outer-core circulation (Bui et al., 2009; Fudeyasu & Wang, 2011). The strength of the outer core is not dependent upon the intensity of the inner core. Rather, it is influenced by the location of the diabatic heating process (Weatherford & Gray, 1988a; Fudeyasu & Wang, 2011).

### 2.2.3 Rainbands

Rainbands, which often spiral outward away from the center of the hurricane, are another important attribute that defines the structure of a hurricane. The inner rainband region of the TC is from the center of the vortex to approximately 150 km radially from the center and the outer rainband region of the TC is from 150 km radially to the extent of the outer-most precipitation (Figure 2.1) (Jiang et al., 2013). The eyewall is the circular band of intense convection that surrounds the eye of the TC and is primarily created by the ascent associated with the secondary circulation (Figure 2.1) (Houze Jr., 2010). Beyond the eyewall is the principal rainband, a band of convection and stratiform rain that spirals inward towards the eyewall and extends to the outer reaches of the inner core region (Figure 2.1) (Didlake & Houze, 2009; Houze Jr., 2010). Formation of the principal rainband is often downshear or downshear left and co-located with precipitation and wind maxima (Willoughby et al., 1984b). The secondary rainbands in the inner core region are smaller, less organized bands of convection that spiral inward toward the eyewall and often connect with either the eyewall or principal rainband (Figure 2.1) (Houze Jr., 2010).

Vortex Rossby waves are understood to be the mechanism that induces the formation of the asymmetric secondary rainbands (Montgomery & Kallenbach, 1997). The vortex Rossby wave theory is the best supported theory for explaining the formation of TC rainbands due to the linkage between the waves and the initial vortex (Montgomery & Kallenbach, 1997).

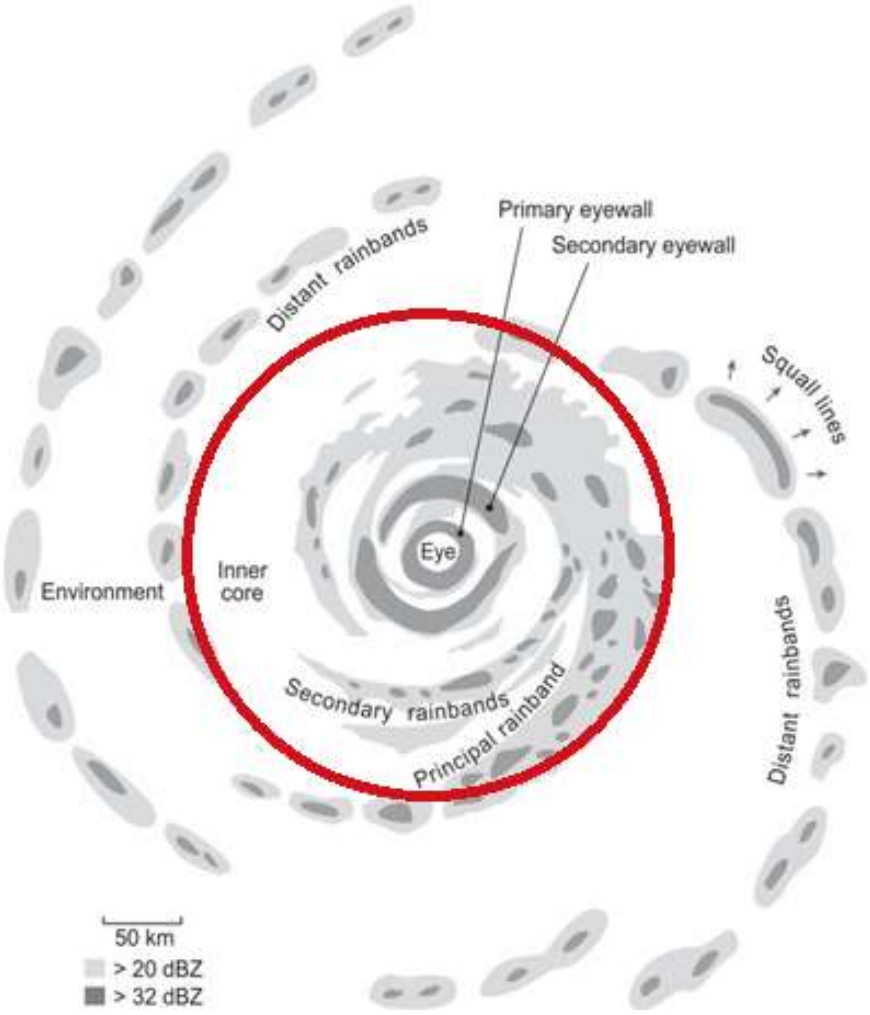


**Figure 2.1:** The inner core, outer core, and precipitation band structure of a tropical cyclone, adapted from Houze (2010). The bold circle distinguishes the inner core from the surrounding environment.

The outer core region of the TC is where the distant rainbands are located (Figure 2.1). Distant rainbands are known to be structurally different than the rainbands in the inner region because the outer region is influenced less by the dynamics of the inner core vortex (Houze Jr., 2010). Convective available potential energy (CAPE) increases as distance from the center of the vortex increases; convective cells in the distant rainbands often form in the areas of increased CAPE values (Molinari et al., 2012). The mature convective cells in the distant rainbands typically have well-pronounced updrafts and downdrafts, which are often much more robust than the convection in the inner region (Houze Jr., 2010). Convective cells in the distant rainbands often form squall lines as the cells mature (Figure 2.1) (Zipser, 1977; Powell, 1990). While the convection in the outer bands of a mature cyclone is often more robust than in the inner region, weaker TCs have been found to have stronger convection in the inner region in comparison with the outer region (Jiang et al., 2013).

### 2.3 Hurricane Landfall

As a hurricane that is moving across the open water approaches land, different physical processes begin to influence the structure and dynamics of the TC. When a TC moves into higher latitudes, features such as midlatitude troughs modify the precipitation structure (Atallah et al., 2007; C. Matyas, 2007), storm motion (Atallah et al., 2007; Zhou et al., 2018), and introduce dry air into the environment (Kimball, 2006). The surface of the land has a higher amount of friction than the ocean's surface, which can reduce the wind speeds of the TC and contribute to the weakening of the storm (Powell, 1987). Surface friction will enhance surface convergence, causing the precipitation to become more asymmetrical (Chan & Liang, 2003; Guo & Matyas, 2016). Moisture availability can lead to asymmetries in the precipitation and convective distributions of a hurricane. Changes in surface roughness and decreased moisture flux

negatively influence the moisture available for the TC to sustain precipitation production (Chan & Liang, 2003). Decreased availability of low-level moisture over the land surface can modify the convective distribution downwind to become more asymmetrical (Chan & Liang, 2003). Dry air intrusion is a process that can affect TC intensity at any point during the storm's life cycle. A modeling study conducted by Kimball (2006) found that dry air has the most influence on a TC when the TC is within close proximity to land. The decreased surface fluxes over the land weaken the strength of the core of the TC, which allows the dry air in the surrounding environment to contribute further to the weakening of the storm and causes an asymmetrical precipitation distribution (Kimball, 2006).

Topographic features are also known to influence the structure of a TC during landfall. Air moving over mountains can influence the intensity and movement of a TC (Leroux et al., 2018). Mountainous terrain influences the structure of a TC's rain shield and convection (C. Matyas, 2007; Villarini et al., 2011). In regions of elevated terrain, specifically the Appalachian Mountains, a TC's rain shield may become concentrated on the left side depending upon the track of the storm with respect to the terrain (C. Matyas, 2007). Matyas (2007) found that the precipitation distribution for TCs that tracked parallel to the Appalachian Mountains was enhanced on the left side while storms that have a track perpendicular to the terrain were enhanced on the right side.

It is important to have a global understanding of how TCs evolve during landfall for the purpose of improving landfall forecasts. Similar to the North Atlantic Ocean basin, the northwest Pacific Ocean basin also experiences TCs, which often make landfall along China's coast. An observational study that included two TCs with slow forward motion found that they had convective distributions similar to that of TCs from the Atlantic basin (Johnny C. L. Chan et al.,

2004). A numerical study found that the landfall direction influences the asymmetrical precipitation distributions of landfalling TCs along the south China coast (Chan et al., 2019). The magnitude of the vertical wind shear is understood to be the most influential factor of asymmetrical precipitation distributions (Chan et al., 2004; Xu et al., 2014).

During landfall, higher precipitation totals are commonly found in the right and front quadrant with respect to the TC center and direction of motion (Johnny C.L. Chan & Liang, 2003); this is characteristic of an asymmetrical precipitation distribution. The precipitation distribution is often asymmetric (symmetric) when the primary circulation is weaker (stronger) (Matyas, 2010). An important variable for predicting the expansiveness of a TCs precipitation field is vertical wind shear (Matyas, 2010). Wind shear that acts against the storm motion causes the TC to have a slower forward speed and higher rainfall rates on the right side of the storm, which further enhances the asymmetrical rain features (Matyas & Cartaya, 2009). Upon landfall, the precipitation shield is known to have a larger spatial extent if the center of the TC remains within close proximity to the coastline (Zhou et al., 2018). TCs with left-side maximums in precipitation are typically undergoing extratropical transition (ET), which occurs when a TC interacts with a strong trough (Atallah et al., 2007). While researchers have considered many factors that influence TC precipitation distributions, only idealized studies have considered the role of atmospheric stability (Johnny C.L. Chan & Liang, 2003; Kimball, 2008).

### 2.4 Heavy Precipitation Factors

Studies in mesoscale meteorology on thunderstorms have previously identified important factors associated with convection. Convection is known to occur in areas where the atmosphere is unstable. Some common measurements for instability are CAPE, K-Index (KI), lifted index (LI), and 700 mb temperatures. CAPE is a measurement of the amount of energy in the

atmosphere that is available for convection to occur. CAPE values greater than 800 J/kg are favorable for convection (Markowski & Richardson, 2010). The KI takes into account vertical temperature lapse rates and the extent of moist air at lower levels of the atmosphere; KI values greater than 35 indicate higher thunderstorm probability (Maddox et al., 1979). The LI is the difference between the 500 mb environmental temperature and the temperature of an air parcel lifted to 500 mb, which will indicate whether an air parcel is warmer or colder than the surrounding atmosphere. LI values less than -4°C indicate that the air parcel is unstable (Schnetzler, 2008). Large-scale convective rainfall events occur when the 700 mb temperatures are less than 12°C, because 700 mb temperatures above 12°C are indicative of the presence of a strong cap, which hinders convective potential of the atmosphere (Junker et al., 1999). Along with instability, high values of precipitable water, approximately 41.66 mm (1.64 in), are necessary for the convective cells to produce heavy precipitation (Junker et al., 1999; Schnetzler, 2008). While the previously stated values for instability and moisture are common measurements for mesoscale convection, the same principals can be applied to the distant rainband region of a TC. This is because the distant rainbands are influenced more by the environment surrounding the TC, which causes the convection in distant bands to be structurally different than the convection closer to the center of the vortex (Houze Jr., 2010).

Observational and modeling studies that have investigated TCs of a similar nature to Hurricane Florence are important in contextualizing this research. In comparison to Hurricane Florence, Hurricane Harvey (2017) was a TC that had very similar storm motion and precipitation characteristics. Each of these TCs produced extreme amounts of precipitation that caused flooding to coastal and inland communities. Both TCs had slow storm motions prior to, during, and after landfall; this is a notable reason as to why the spiral rainbands trained over a

small area for an extended period of time. Hurricane Beulah (1967) is another interesting storm that made landfall in southern Texas. Upon landfall, the storm weakened and eventually stalled over southern Texas, producing 254-508 mm (10-20 in) of rain across the region, local amounts exceeded 762 mm (30 in) (Sugg & Pelissier, 1968). In 2003, Tropical Storm Allison moved slowly across southeastern Texas, producing 254-508 mm (10-20 in) of precipitation from southeastern Texas to southern Louisiana (Stewart, 2001). Hurricane Florence is one of many recent TCs that has slowed down during landfall and produced significant precipitation.

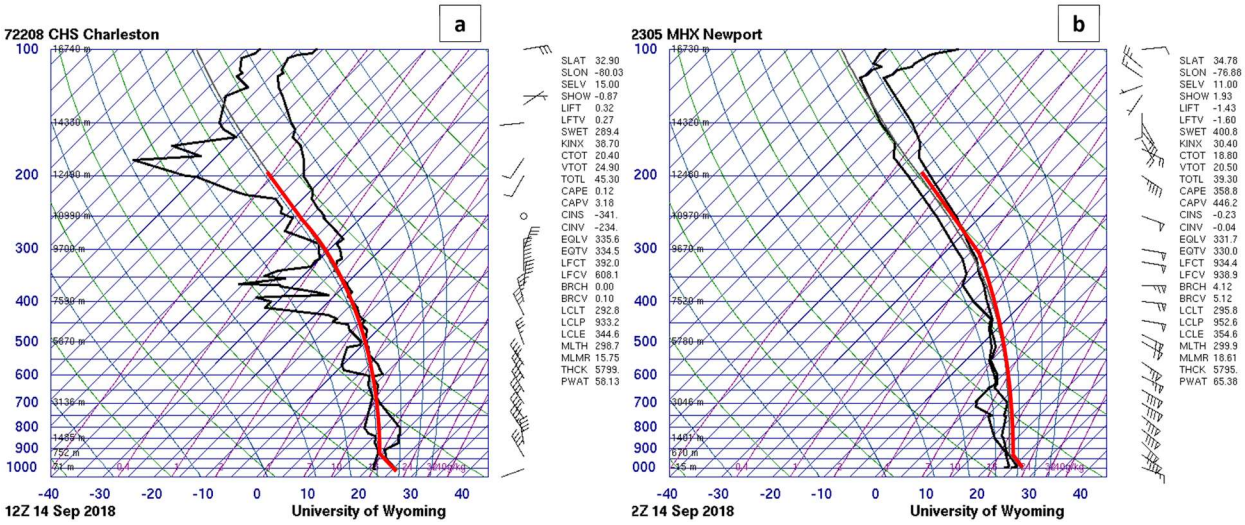


**Figure 2.2:** Skew-T diagrams showing atmospheric profiles of air temperature, dew point temperature, and air parcel temperature (red line) from the left side (A) and right side (B) of Hurricane Florence's storm track. Sourced from the University of Wyoming Weather Web. (http://weather.uwyo.edu/upperair/sounding.html)

The role of land surface conditions has been known to influence the intensity of landfalling TCs. A previous study used high-resolution Advanced Research Weather Research and Forecasting (WRF-ARW) simulations to determine that anomalously high soil moisture contributed to the re-intensification of Tropical Storm Erin (2007) after landfall (Kellner et al.,

2012). Land surface variables, such as soil moisture and surface roughness, are known to have significant impacts on the intensity of TCs upon landfall (Kishtawal et al., 2012). Similar logic can be applied to Hurricane Florence by considering how the moisture value within land cover parameters influences the atmospheric stability during and after landfall. Based on observations (Figure 2.2), on the left side of the TC track during landfall, there was a more stable, saturated air mass (Figure 2.2A). The right side of the TC had a moist boundary layer and increased instability during landfall (Figure 2.2B), which supported robust convection and heavy precipitation. Hypothetically, a drier land surface should cause the air mass to have a drier vertical profile as it circulates over land, and once the air mass moves back over the warm, moist ocean surface the instability will increase, forming robust convection and strong asymmetry in precipitation. On the other hand, a more moist land surface will cause the air mass to have a mostly saturated vertical profile over land, and the introduction of moisture from the ocean surface will sustain a moist adiabatic profile with little instability to fuel robust convection in the distant rainband region.

A better understanding of hurricane formation, landfall, and heavy precipitation formation leads to the present gap in the literature. Instability and heavy precipitation are well-known topics in mesoscale meteorology and understood to occur in TC rainbands during landfall. However, such convective features have yet to be appropriately documented for TCs during landfall. This study will utilize numerical weather modeling to simulate Hurricane Florence (2018) and investigate the convective distribution associated with the distant rainbands during landfall.

# Chapter 3: Methods

## 3.1 WRF Model

Numerical weather modeling is a useful tool that allows researchers to simulate realistic and idealized atmospheric conditions to better understand how TCs evolve under specific conditions (e.g., Chan & Liang, 2003; Kimball, 2006; Yang et al., 2019). The numerical model implemented for this study is the Advanced Research Weather Research and Forecasting (WRF-ARW) version 3.6.1 (Skamarock et al., 2008). The WRF-ARW offers an open-source platform for community members to use, write, and improve the WRF code, which creates a collaborative community that fosters unique, reproducible research studies. The WRF-ARW solver utilizes non-hydrostatic Euler equations (Skamarock et al., 2008). Non-hydrostatic models are specifically useful for forecasting vertical motion at a relatively small scale which will be especially important for simulating the convective precipitation in the outer rainbands of Hurricane Florence. The Advanced Hurricane WRF (HWRF) has exhibited the ability to model wind and precipitation asymmetries in the 48-72 hour forecast range (Davis et al., 2008).

The Noah land surface model (LSM) is an integral component of WRF because it includes the influence of surface layer schemes such as land cover, soil moisture, and snow cover (Skamarock et al., 2008) and initializes the state of the planetary boundary layer (PBL) (F. Chen & Dudhia, 2001). The Noah LSM itself may be used in numerous types of research. For example, some researchers use the model to integrate coarse resolution soil data into studies to improve hydrological models. Specifically, a study found the Noah LSM soil moisture parameter to be effective for hydrological modeling at local scales (Srivastava et al., 2013). The LSM is also applied to studies on climate change impacts. Vahmani and Hogue (2014) utilized the Noah LSM-single layer urban canopy model (SLUCM) parameters to determine the effects of urban

irrigation on local hydrological cycles. Simulations involving changes in soil and roughness parameters have found that TC intensity is sensitive to changes in the PBL (Evans et al., 2011).

TC landfall forecasts have greatly improved as the research and forecasting communities have learned more about how the TC's track and precipitation are influenced by the terrain and the surrounding environment (e.g., Xu et al., 2014; Leroux et al., 2018). Past numerical weather modeling research identified convective asymmetries associated with TC landfall (Chan & Liang, 2003). A recent study using the WRF-ARW found that the extreme rainfall produced from Hurricane Harvey (2017) was a result of the convective distant rainbands that made landfall (Yang et al., 2019). Advancements in NWP have improved the accuracy of 3-day intensity and track forecasts, but beyond three days, intensity forecasts become less accurate due to limitations with the model's ability to forecast the track of the TC (Leroux et al., 2018). Altering LSM parameters within the WRF-ARW can provide opportunities for modeling TC landfall. A study that altered the LSM parameter for soil moisture found that anomalously wet soil can provide enough moisture for a simulated TC to re-intensify upon landfall (Kellner et al., 2012). Advancements in TC research and forecasting using the WRF-ARW make the model an ideal tool for this study of Hurricane Florence.

### 3.2 Model Configuration

In this study, I first generate a control simulation (CTRL) of Hurricane Florence during landfall on the coast of North Carolina, and then test my hypotheses further by conducting two experimental simulations. All simulations will use a two-way interactive nested grid. In order to simulate the large-scale features of the atmosphere, the outer domain has a resolution of 18 km and encompasses the continental United States (CONUS) and North Atlantic Ocean (Figure 3.1).

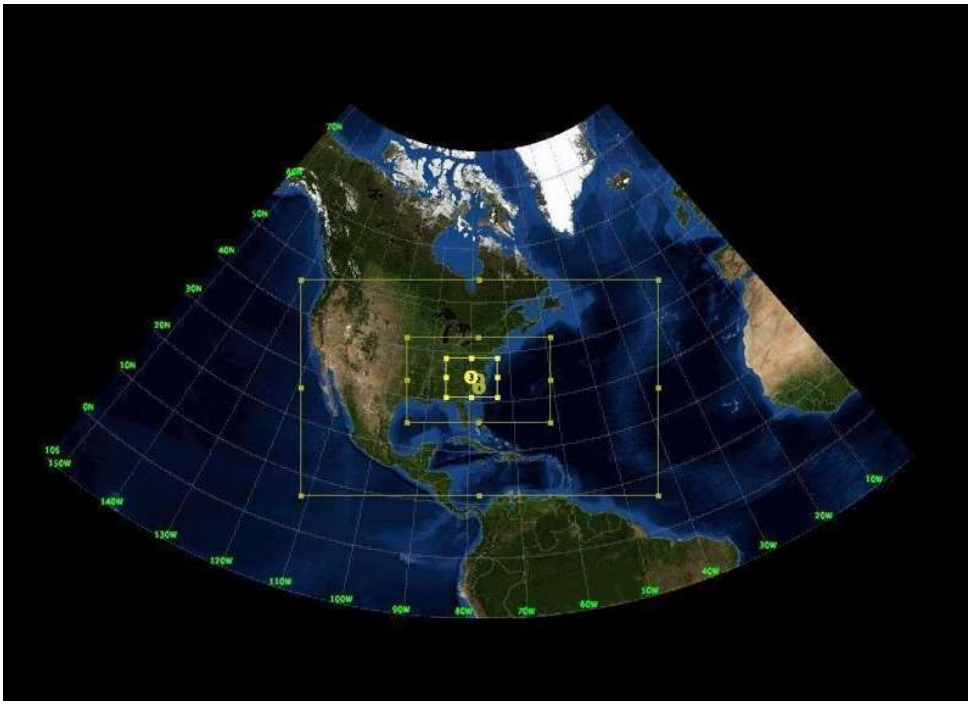

**Figure 3.1:** Nested domain structure used for the CTRL and experimental simulations. The largest domain has a resolution of 18 km, followed by 6 km and 2 km nests.

Finer resolution nests of 6 km and 2 km are fitted into the domain to focus on the East Coast and North Carolina, respectively. The vertical resolution of the WRF-ARW has 40 vertical levels from the surface to 5 mb. The initial conditions for the simulations are obtained from the final analysis of the Global Forecast System (GFS). The GFS final analysis has a gridded spatial resolution of 1.0° and a temporal resolution of 6 hours. Best track data for Hurricane Florence, sourced from the Atlantic hurricane database (HURDAT2), will be compared with the results of CTRL to ensure the simulation is an accurate representation of the observed hurricane track and intensity. Hurricane Florence precipitation estimates are sourced from the Stage IV (ST4) dataset, a composite of NOAA Next-Generation Radar (NEXRAD) estimates and rain gauge data from the National Weather Service (NWS) River Forecast Centers (RFCs) and the National Centers for Environmental Prediction (NCEP). Physical parameterizations that are commonly

used to simulate real TCs are employed (Table 3.1) (Skamarock et al., 2008). The Noah LSM in CTRL will utilize the land use categories defined by the International Geosphere-Biosphere Programme (IGBP) and derived by the Moderate Resolution Imaging Spectroradiometer (MODIS) satellite instrumentation.

| **Physical Parameterization** | **WRF-ARW v. 3.6.1 option** |
|---|---|
| Cumulus | Kain-Fritsch (18-km domain only) |
| Microphysics | WRF single-moment 6-class (WSM6) |
| Longwave Radiation | Rapid Radiative Transfer Model |
| Shortwave Radiation | Rapid Radiative Transfer Model |
| Planetary Boundary Layer | Yonsei University |
| Surface Layer | Revised MM5 surface layer scheme |
| Land Surface | Noah Land Surface Model |

**Table 3.1** Physical Parameterizations

In order for CTRL to be viable, the simulated TC must possess features that are similar to the actual hurricane. To establish this, I will visually compare the simulated TC track and intensity with the best track data to ensure that the simulation is similar to the actual event. The precipitation totals will be compared to ensure that the simulated TC produces similar rainfall totals and rainfall patterns. Air parcel stability on each side of the TC track will be examined using skew-T diagrams and CAPE calculations. CAPE will indicate air parcel buoyancy and, therefore, indicate if and where enhanced instability is located surrounding the TC. These results will be compared with the simulated precipitation totals to determine if there is a significant relationship between the variables. This framework will address the influence of atmospheric stability on the asymmetrical precipitation distribution.

### 3.3 Noah Land Surface Model

The CTRL utilizes land-use categories sourced from the modified IGBP MODIS 20-category land use dataset. The spatial distribution of the modified IGBP MODIS 20-category

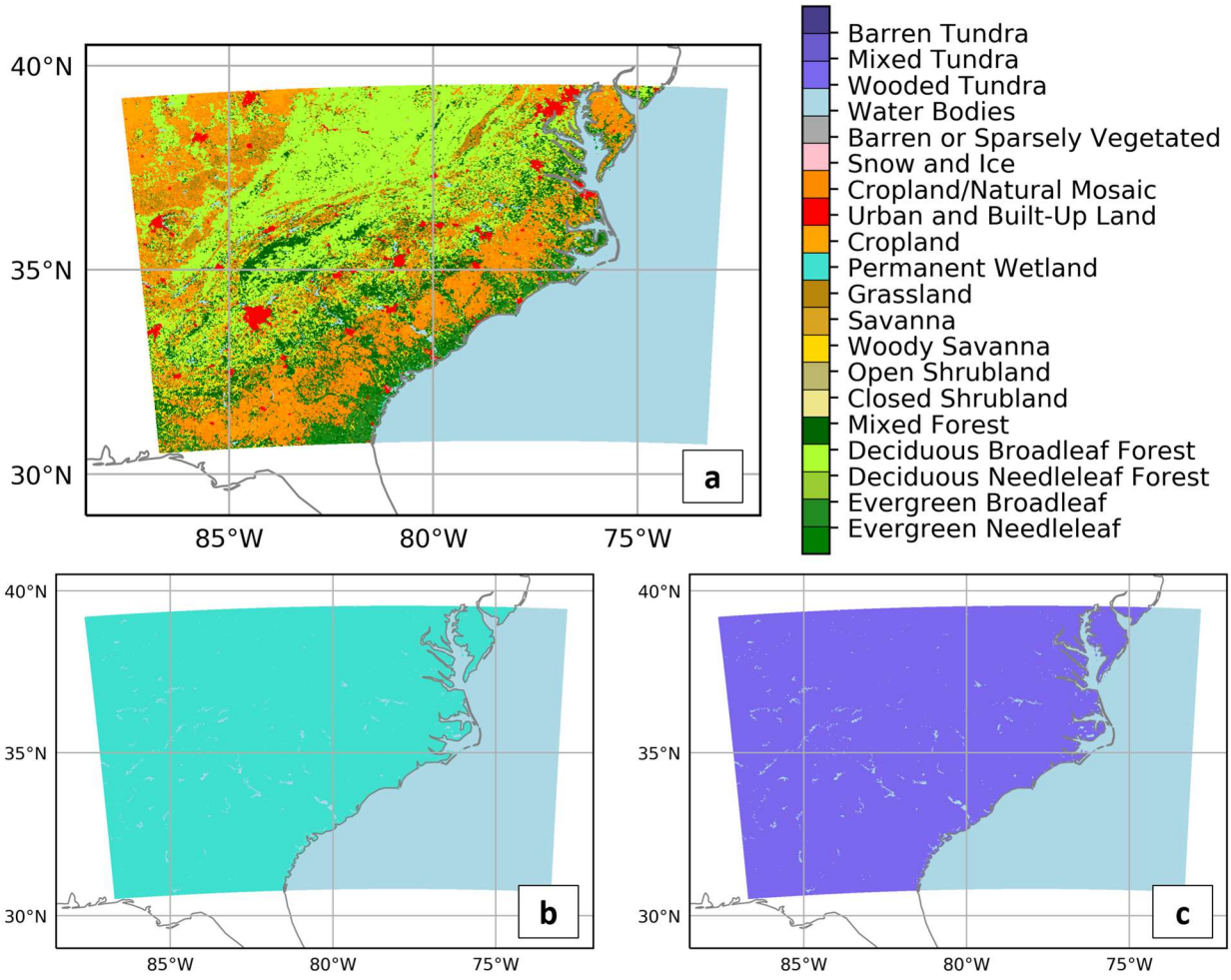


**Figure 3.2** (a) Modified IGBP MODIS 20-category land-use data for the CTRL, (b) LU11 (permanent wetland), and (c) LU18 (wooded tundra) 2-km horizontal resolution domains.

land use scheme for the 18 km domain is displayed in Figure 3.2. Table 3.2 summarizes the modified IGBP MODIS land-use types and important variables for each land use type in the WRF domain. Background roughness length ($Z_0$) is a parameter that is utilized by the boundary layer parameterization scheme to predict the horizontal mean wind speeds near the surface. In

simple terms, the length represents a measure of the surface roughness (Stull, 2012). The variable $Z_{0,min}$ in Table 3.2 defines the minimum background roughness length throughout the year measured in meters, whereas the variable $Z_{0,max}$ indicates the maximum background

| Land Use Index | Count | Percentage | Z0min (m) | Z0max (m) | HS |
|---|---|---|---|---|---|
| 1 - Evergreen Needleleaf Forest | 7413 | 15.97 | 0.5 | 0.5 | 47.35 |
| 2 - Evergreen Broadleaf Forest | 2702 | 5.82 | 0.5 | 0.5 | 41.69 |
| 3 - Deciduous Needleleaf Forest | 1 | 0.00 | 0.5 | 0.5 | 47.35 |
| 4 - Deciduous Broadleaf Forest | 2508 | 5.40 | 0.5 | 0.5 | 54.53 |
| 5 - Mixed Forests | 5268 | 11.35 | 0.2 | 0.5 | 51.93 |
| 6 - Closed Shrublands | 99 | 0.21 | 0.01 | 0.05 | 42 |
| 7 - Open Shrublands | 6708 | 14.45 | 0.01 | 0.06 | 39.18 |
| 8 - Woody Savannas | 1258 | 2.71 | 0.01 | 0.05 | 42 |
| 9 - Savannas | 286 | 0.62 | 0.15 | 0.15 | 54.53 |
| 10 - Grasslands | 8746 | 18.84 | 0.1 | 0.12 | 36.35 |
| 11 - Permanent wetlands | 24 | 0.05 | 0.3 | 0.3 | 55.97 |
| 12 - Croplands | 6552 | 14.12 | 0.05 | 0.15 | 36.25 |
| 13 - Urban and Built-Up | 455 | 0.98 | 0.5 | 0.5 | 999 |
| 14 - Cropland/natural vegetation mosaic | 3098 | 6.67 | 0.05 | 0.14 | 36.25 |
| 15 - Snow and Ice | 1 | 0.00 | 0.001 | 0.001 | 999 |
| 16 - Barren or Sparsely Vegetated | 373 | 0.80 | 0.01 | 0.01 | 999 |
| 17 - Water Bodies | 0 | 0.00 | 0.0001 | 0.0001 | 51.75 |
| 18 - Wooded Tundra | 886 | 1.91 | 0.3 | 0.3 | 42 |
| 19 - Mixed Tundra | 40 | 0.09 | 0.15 | 0.15 | 42 |
| 20 - Barren Tundra | 0 | 0.00 | 0.05 | 0.1 | 42 |

**Table 3.2** Modified IGBP MODIS 20-category land-use data for the 18-km nested domain. The count column indicates the total number of cells for each land-use index within the 18-km domain, and the percentage column indicates the areal percentage of each land-use category within the domain. The vegetation parameter columns for HS, $Z_{0,min}$ , and $Z_{0,max}$ represent the values associated with each land-use category, respectively.

roughness length throughout the year in meters. In Table 3.2, the variable HS is a parameter used in the vapor pressure deficit function, and it represents the moisture associated with the vegetation for a given land use type (Mitchell, 2005). Further information about other variables

associated with the land-use types can be found on the National Center for Atmospheric Research website (NCAR 2012) or in Mitchell (2005).

The CTRL values for $Z_{0,min}$, $Z_{0,max}$, and HS in Table 3.3 were determined by averaging each vegetation parameter based on the land-use index counts from Table 3.2. The influence of land-use category 17 (water bodies) is excluded from the variable averages for the CTRL in Table 3.3 because the influence of the water bodies remains the same amongst all the experiments. The mean $Z_{0,min}$ is 0.27 m and the mean $Z_{0,max}$ is 0.35 m for the CTRL (Table 3.3). The mean HS for the CTRL is 46.44 (Table 3.3). The average for HS excludes land-use categories 13, 15, and 16 due to each category having a HS value of 999.0, as well as the effect of water bodies since the influence of water bodies remains the same in all experiments (Table 3.2). The vegetation parameter, HS, is isolated in the experimental simulations in order to determine if any relationship exists between low-level moisture and the distributions of stability and of precipitation around the simulated TCs.

| Experiment | $Z_{0,min}$ (m) | $Z_{0,max}$ (m) | HS (Moisture) |
|---|---|---|---|
| Control (CTRL) average | 0.27 | 0.35 | 46.44 |
| Permanent Wetland (LU11) | 0.30 | 0.30 | 55.97 |
| Wooded Tundra (LU18) | 0.30 | 0.30 | 42.00 |

**Table 3.3** Land use parameters for CTRL, LU11, and LU18 experiments. For the CTRL experiment, these values represent spatial averages based on the 2-km domain. For the LU11 and LU18 experiments, these are IGBP MODIS land use parameter values for permanent wetland and wooded tundra land use categories, respectively.

### 3.4 Experimental Design

In addition to the CTRL, two experimental simulations will be examined to determine how the surface moisture availability influences the asymmetrical precipitation distribution

during landfall. The experimental simulations will be performed by altering the land surface cover to be moister or drier. The land surfaces selected for the experimental simulations are herbaceous wetland and wooded tundra because these land cover classes have the same $Z_{0,min}$ and $Z_{0,max}$ (0.3 m) and different low-level moisture availability (HS) (Table 3.3). The constant $Z_0$ values will limit changes to the wind fields, thus isolating the impact of HS on the experimental TCs. The first experimental simulation will change the land surface cover to herbaceous wetland (LU11), which is hypothesized to create a moister land surface and result in a symmetrical precipitation distribution. indicating increased moisture may sustain the convective structure of the TC during the landfall period. The second experimental simulation will alter the land surface cover to wooded tundra (LU18), which is hypothesized to decrease the low-level moisture availability and cause an asymmetrical precipitation distribution. The results of the experimental simulations will be compared to CTRL to determine if significant differences exist. TC tracks and intensities will be examined to determine if the strength of the inner core is impacted by the altered land surfaces. Symmetry of the precipitation distributions will be analyzed using storm-total and daily accumulation to further explore the effects of low-level moisture availability. Simulated CAPE will be used to compare stability for static locations right- and left-of-track; these results will determine how stability varies with respect to the TC track. The impact of the altered land surfaces on spatial variations in low-level relative humidity and CAPE will also be examined to further understand how the experiments impact moisture and stability. The results from the experimental simulations will address the second research objective by investigating the influence of altered land cover on atmospheric stability and the resulting precipitation distribution.

## Chapter 4: Control Simulation Results

This chapter compares the observations from Hurricane Florence to the CTRL. The goal of this chapter is to highlight Hurricane Florence's precipitation asymmetries and address the spatial variability of stability surrounding the TC during the landfall period. Track and intensity comparisons with observations will be used to illustrate the viability of CTRL. Precipitation accumulation is examined for asymmetries and used as further justification of the importance of the period of slow storm motion during landfall. Atmospheric stability is explored spatially to provide an understanding of how stability varies surrounding the TCs. The results of this chapter will introduce further questions on how precipitation asymmetries are influenced by the TCs surrounding environment.

### 4.1 Track and Intensity Verification

Before addressing the research questions, it is important to compare the CTRL with observations to verify that the simulated TC track, intensity, and structure are consistent with observations. The track is determined by the location of the minimum mean sea level pressure ($MSLP_{min}$) during each 1-hour time-step. Figure 4.1a displays the observed track for Hurricane Florence compared to the track in CTRL. Both tracks are well aligned until landfall, when the CTRL TC begins to move slightly north compared with the best track. The intensity of the simulated TC is measured by the $MSLP_{min}$ (hPa) and maximum sustained 10-m wind speeds (knots). In the CTRL, the TC is initialized with a higher $MSLP_{min}$ and weaker sustained 10-m wind speeds than the best track due to the lower resolution GFS analyses that were used for initial conditions. After initialization, CTRL TC is a Category 2 hurricane (based on the Saffir-Simpson Hurricane Wind Scale) with sustained 10-m wind speeds between 83 and 90 knots from 09 UTC 13 September to 06 UTC 14 September. The CTRL TC sustained 10-m

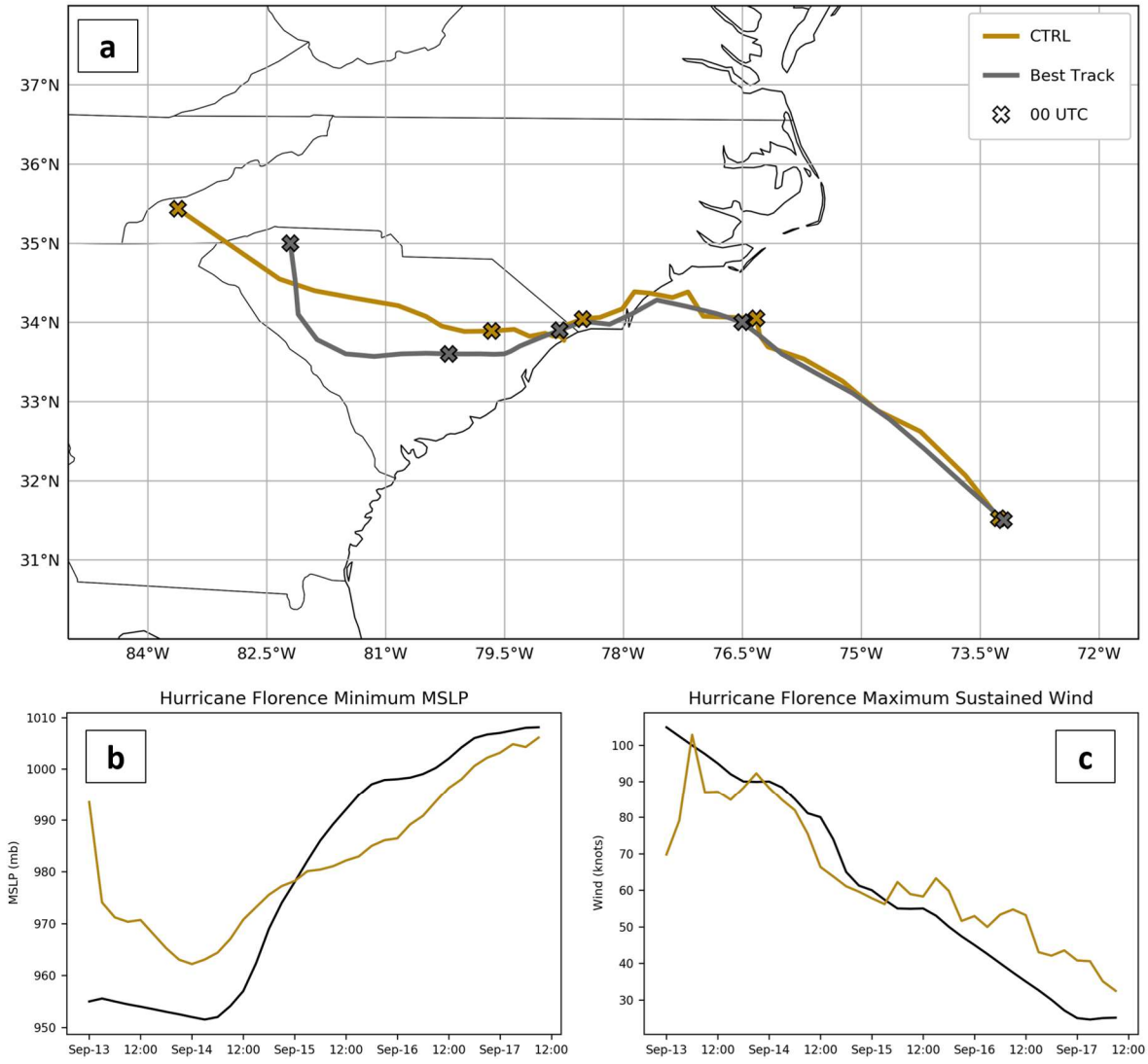


**Figure 4.1** Best track position and intensity data compared to the CTRL for (a) storm track, (b) $MSLP_{min}$ (mb), and (c) maximum sustained 10-m wind (knots). All plots correspond to data beginning 00 UTC September 13 and ending 09 UTC September 17. Track (a) includes X markers every 24 hours at 00 UTC.

winds quickly weaken to Category 1 strength after 06 UTC 14 September and maintains that intensity through 18 UTC 14 September. During the same period the tracks are nearly identical (Figure 4.1a), showing the CTRL simulates a similar period of slow storm motion parallel to the coast during the landfall period. From 03 UTC 15 September through the end of the simulation at

09 UTC 17 September, the CTRL TC's wind speeds were greater than best track, indicating a slightly stronger TC than the actual storm. During the same period, the CTRL track diverges slightly from the best track (Figure 4.1a). The $MSLP_{min}$ for the CTRL reaches its lowest value of 965 mb at 00 UTC 14 September, indicating the presence of a strong low-pressure system. After 00 UTC 14 September, the $MSLP_{min}$ for the CTRL slowly increases for the remainder of the simulation. At 00 UTC 15 September, the $MSLP_{min}$ for the CTRL and best track meet at about 980 mb. Overall, the CTRL TC intensity and track match well with observations, which is expected since the model initial and boundary conditions are provided by an analysis rather than a forecast.

### 4.2 Precipitation Comparisons

A prominent feature of Hurricane Florence was the asymmetrical distribution of precipitation. This asymmetry is first examined using the accumulated precipitation from 00 UTC 13 September through 09 UTC 17 September for the 4 km resolution ST4 data and 2 km resolution CTRL output (Figure 4.2). Figure 4.2 also shows the location of landfall, denoted by the "X", and the locations for two NWS upper air observation sites, which will be discussed further in the Atmospheric Stability section later in the chapter. According to ST4 data,

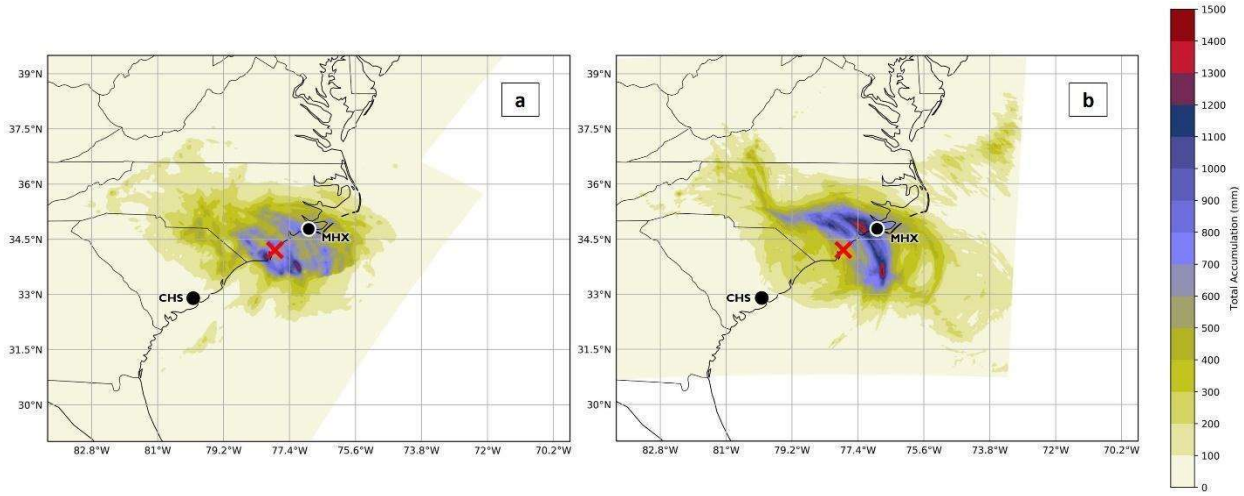


**Figure 4.2** Accumulated precipitation starting at 00 UTC 13 September 2018 and ending at 09 UTC 17 September 2018 for (a) ST4 and (b) CTRL. CHS and MHX stations are overlaid.

Hurricane Florence produced an estimated storm-total rainfall maximum of approximately 1465 mm over the ocean and approximately 1100 mm over land (Figure 4.2a). The ST4 estimates have a sharp cut-off over the ocean, which illustrates the spatial extent of the NEXRAD network. It is important to note that the accuracy of the NEXRAD reflectivity algorithms decrease farther away from the radar location (Ryzhkov & Zrnic, 1995). The CTRL simulated a storm-total maximum accumulation of 1466 mm over ocean and approximately 1400 mm over land (Figure 4.2b). Compared with ST4, the CTRL produced a longer swath of higher precipitation totals, typical of training rainbands (Figure 4.2b). Overall, both the estimates from ST4 and CTRL display asymmetries in the storm total accumulations.

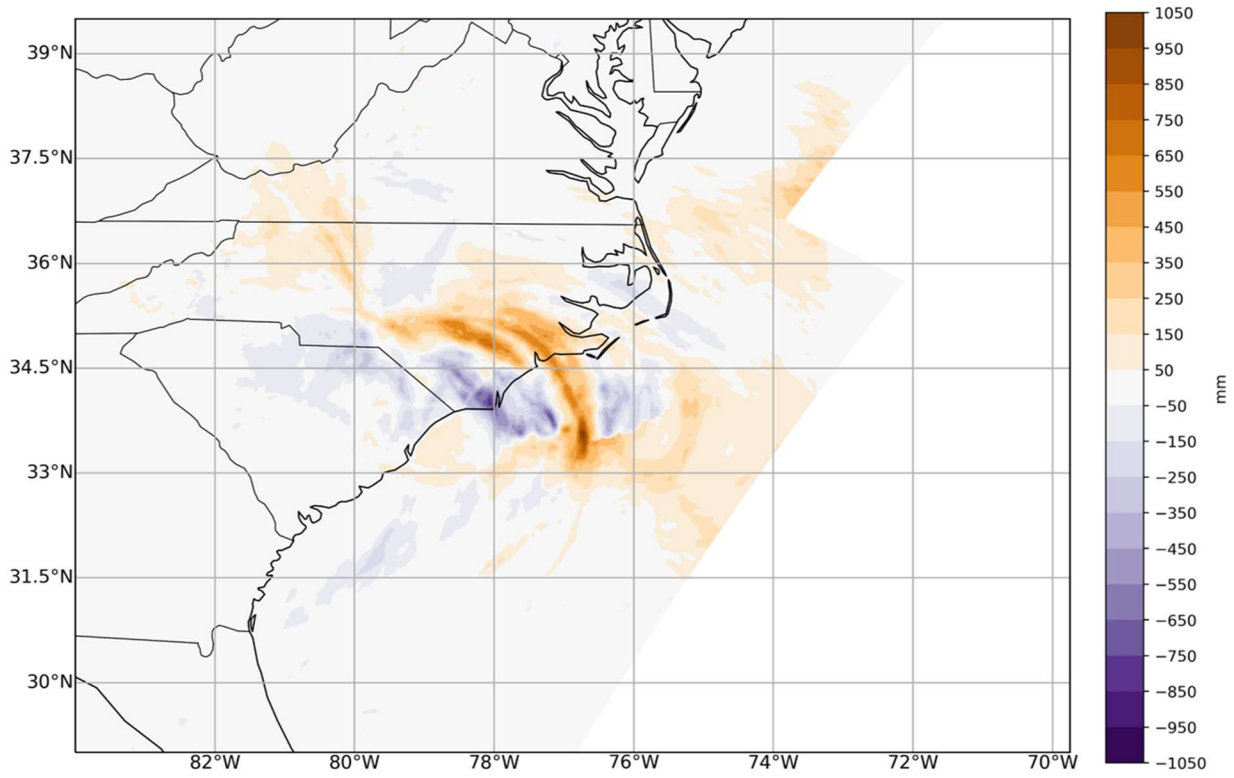


**Figure 4.3** Storm-total rainfall differences between CTRL and ST4 in mm. Positive (negative) values indicate the CTRL simulated more (less) rainfall than ST4.

In order to compare differences in total precipitation between CTRL and ST4, the CTRL accumulation was re-gridded to 4 km resolution to match the spatial resolution of ST4. Total rainfall differences were then calculated as shown in Figure 4.3, where positive (negative) values signify CTRL simulated more (less) rainfall than ST4. Differences show that CTRL overestimates a long band of higher totals right-of-track, with a maximum difference of 1022 mm occurring over ocean (Figure 4.3). The minimum precipitation difference (-802 mm) (Figure 4.3) shows the CTRL under simulates the magnitude of precipitation that occurs closer to the TC center near the NC-SC border (see track in Figure 4.1a). Although there are differences in representation of the intensity of the banded feature, the rainfall pattern for CTRL is comparable

to ST4 in terms of spatial coverage. Investigation of the relationship between rainband intensity and atmospheric stability will be discussed in detail later in this chapter.

Daily precipitation accumulation for 14 September through 16 September for the ST4 and CTRL are used to determine which days have the strongest asymmetry in precipitation (Figure 4.4). Both the real and simulated TCs begin to interact with land around 11 UTC on 14 September, leading the precipitation to have a similar spatial extent and an asymmetrical distribution of daily rainfall on 14 September (Figure 4.4a-b). The maximum rainfall accumulation on 14 September is 482 mm for CTRL and 601 mm for ST4 (Figure 4.4a). The ST4 estimates of daily accumulation on 14 September (Figure 4.4a) indicate that a considerable amount of precipitation fell within the inner core region of the TC. Precipitation asymmetries often form downshear and downshear left during landfall where vertical wind shear exists (Chan et al., 2004; Xu et al., 2014). According to data from the Statistical Hurricane Intensity Prediction Scheme (SHIPS; Demaria & Kaplan, 1994, 1999), the mid-level (850-500 mb) vertical wind shear is weak (6.6 knots) out of the northwest (Figure 4.4a). The CTRL simulated higher totals farther away from the TC track on 14 September and under-simulated the intense precipitation within the inner core during this time period (Figure

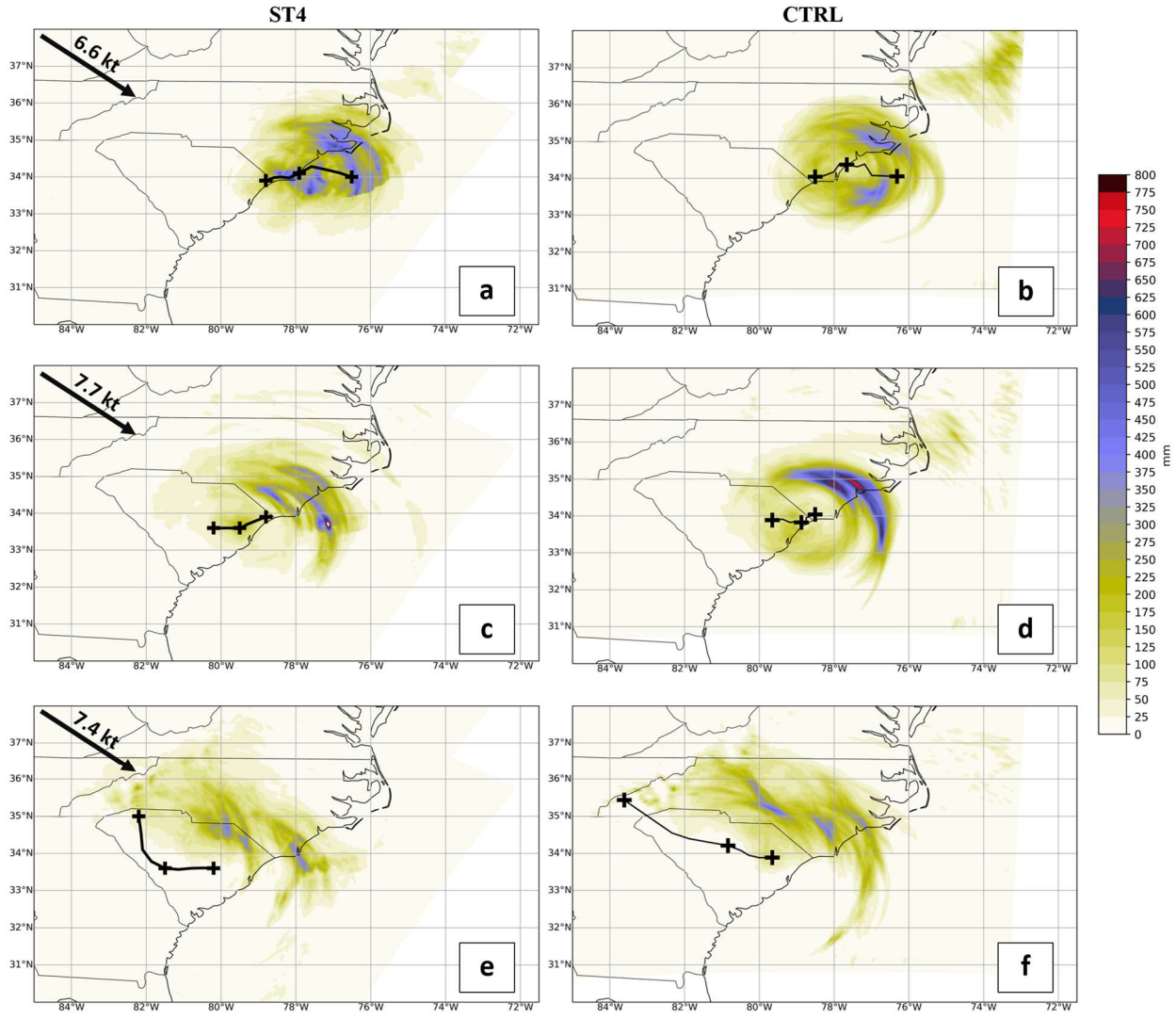


**Figure 4.4** Daily accumulated precipitation (mm) for ST4 (left) and CTRL (right) for (a-b) 14 September (c-d) 15 September, and (e-f) 16 September. TC tracks and center positions are overlaid with a plus sign (+) for 00 UTC and 12 UTC positions. SHIPS daily average mid-level (850-500 hPa) vertical wind shear direction (arrow) and magnitude are indicated in the ST4 (left) plots.

4.4b). Daily accumulation for 14 September is asymmetrical for both TCs, yet it is important to look at how the asymmetry evolves as the TC positions allow for land-ocean interaction on 15 September.

During the 15 September accumulation period, the TCs continued a prolonged period of slow storm motion parallel to the coastline (Figure 4.1a), and asymmetries became more pronounced for both ST4 (Figure 4.4c) and CTRL (Figure 4.4d). The ST4 daily accumulation shows three distinct bands of higher precipitation totals occurring right-of-track with the maximum (996 mm) occurring off-shore (Figure 4.4c). On this day, the average mid-level vertical wind shear was weak (7.7 knots) out of the northwest (Figure 4.4c), possibly contributing to the formation of asymmetries. The CTRL simulated two distinct bands of higher precipitation totals right-of-track with the maximum (747 mm) occurring over land and beyond the influence of the inner core (Figure 4.4d). Lower precipitation totals occur farther inland and left-of-track for both ST4 (Figure 4.4c) and CTRL (4.4d). The accumulation has well defined asymmetry while the TCs are stationary near the coast, but the next 24-hour period should be examined to determine how the asymmetry evolves after this period of slow motion.

As the TCs begin to move farther inland, the asymmetry continues to be observable and accumulation becomes more widespread across most of the domain. On 16 September, the precipitation accumulation for both TCs occurs predominantly right-of-track (Figure 4.4e-f), leading to apparent asymmetry in the precipitation distribution. Mid-level vertical wind shear on 16 September is weak (7.4 knots) and out of the northwest (Figure 4.4e), which likely contributes to the asymmetry. The widespread spatial distribution of the rainfall accumulation on 16 September is due to the influence of the land surface as the TCs moved further inland and increased speed, as denoted by the larger separation between the 12 UTC 16 September and 00 UTC 17 September center locations in Figure 4.4e-f. The accumulation and track for 16 September show that the 24-hour period is past the period of slow storm motion, indicating

asymmetries could primarily be attributed to influences of storm motion, vertical wind shear, land surface, topography, or other physical factors.

The daily accumulation shows that similar accumulation asymmetries occur in both the ST4 and CTRL between 14 September and 16 September, a time period in which both TCs move very slowly along the coast (Figure 4.1). In order to address my first research question, I will limit the temporal scale to 00 UTC 14 September through 12 UTC 16 September when the TC is nearly stationary around the time of landfall. Doing so should limit asymmetries that develop due to TC motion and shear, and focus on those that form due to land-ocean forcing mechanisms.

### 4.3 Atmospheric Stability

The atmospheric stability for the CTRL is verified by comparing NWS upper air sounding observations with model-derived soundings from the CTRL. The NWS locations are chosen based on their proximity to the location where Hurricane Florence made landfall at 1115 UTC 14 September 2018. Charleston, South Carolina (CHS) (32.9°N, -80.03°W) is located left-of-track while Newport/Morehead City, North Carolina (MHX) (34.78°N, -76.88°W) is located right-of-track. CHS is located within the outer rainband region of the TC at approximately 250 km from the location of landfall, a prime spot to verify the stability of air masses moving off-shore. MHX is located approximately 106 km from the location of landfall (Figure 4.2), which is on the fringe of the 100 km average extent of the inner rainband region of the TC (Jiang, Ramirez, and Cecil 2013). The location of MHX provides an ideal position to better understand the stability right-of-track. Observations and simulated 12-hourly CAPE (Table 4.1) and convective inhibition (CIN) (Table 4.2) are examined to evaluate atmospheric stability. Higher CAPE indicates an air parcel will rise while higher CIN prevents an air parcel from rising.

The skew-T diagrams in Figure 4.5 compare the vertical atmospheric profiles from CHS and MHX with the CTRL simulation at 12 UTC 14 September 2018, the closest observation to

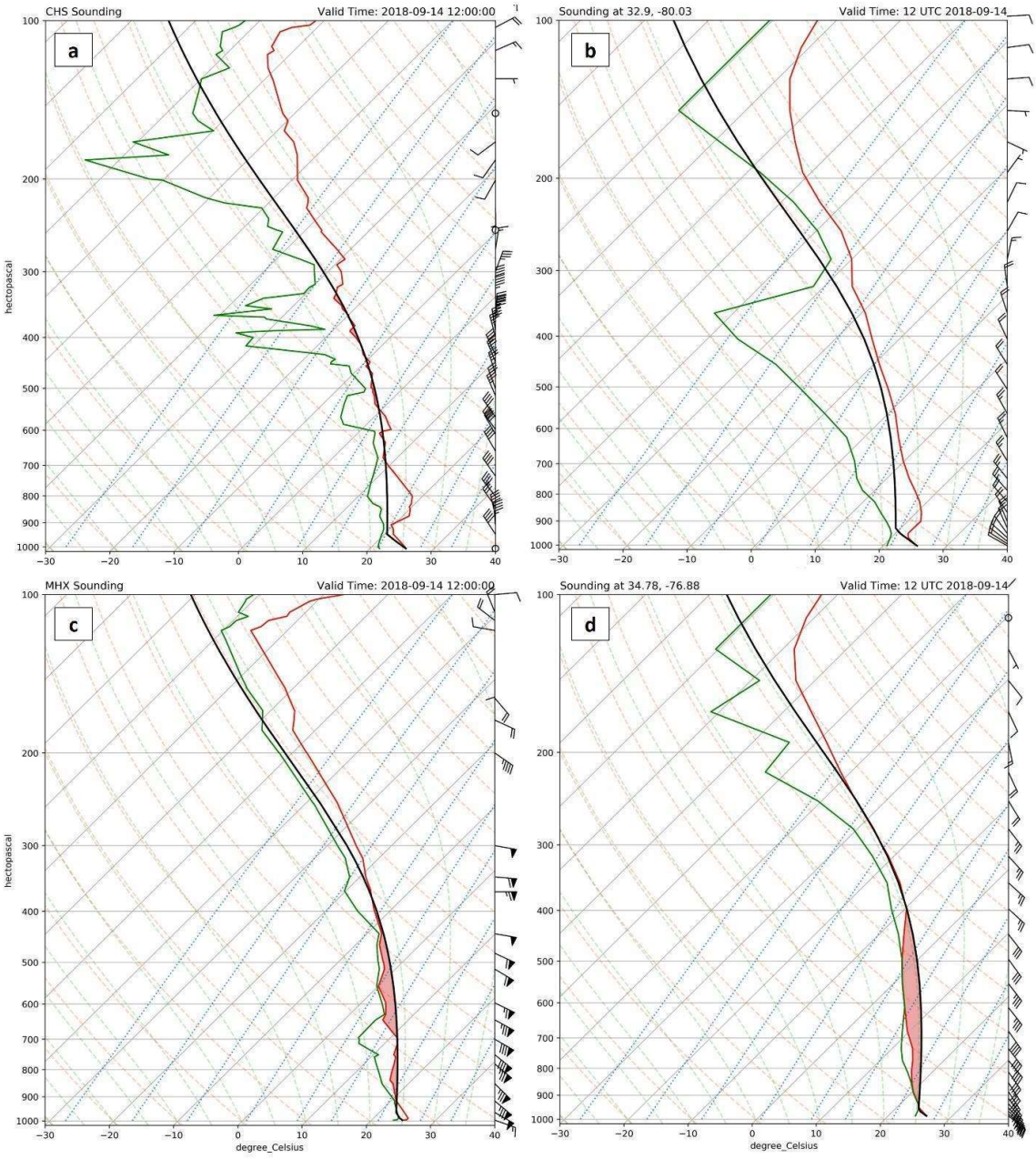


**Figure 4.5** Sounding profiles at 12 UTC 14 September 2018 for the observed (left) and CTRL (right) at the (a-b) CHS location (32.9°N, -80.03°W) and (c-d) the MHX location (34.78°N, -76.88°W). CAPE (J $kg^{-1}$) is shaded in red where it exists.

the time of landfall. The CHS sounding (Figure 4.5a) shows a dry, stable atmosphere; at this time, the CAPE is 6.82 J $kg^{-1}$ (Table 4.1) and CIN is -217.82 J $kg^{-1}$ (Table 4.2). The vertical wind profile from 950 hPa to 550 hPa at CHS (Figure 4.5a) shows nearly unidirectional flow from the northwest around 40 knots at the surface with a gradual shift to northerly flow above 550 hPa. Similar to the CHS observation (Figure 4.5a), the CTRL sounding (Figure 4.5b) shows a dry, stable sounding profile. The vertical wind profile from 950 hPa to 400 hPa for the CTRL (Figure 4.5b) shows northwest flow between 20 knots and 25 knots near the surface veering to northerly flow above 400 hPa. CAPE for CTRL at the CHS location was 0.0 J $kg^{-1}$ (Table 4.1) and CIN was 0.0 J $kg^{-1}$ (Table 4.2), which verifies that the CTRL left-of-track stability is comparable to the observations.

The MHX sounding (Figure 4.5c) shows a moist, unstable atmosphere right-of-track as the air mass moved on-shore. The CAPE observed at MHX was 226.42 J $kg^{-1}$ (Table 4.1), and CIN was -2.06 J $kg^{-1}$ (Table 4.2). These observations are consistent with a tropical oceanic air mass, which tends to be moist adiabatic with minimal CIN (Dunion, 2011). Additionally, CAPE within 400 km of a TC tends to be higher in downshear quadrants (Molinari et al., 2012). At this time, mid-level (850-500 mb) vertical wind shear is weak and northwesterly (Table 4.3). Note that shear must be calculated with the TC removed, so the vertical wind profiles at CHS and

| **CAPE $\frac{J}{kg}$** | **Left-of-track** | | **Right-of-track** | |
|---|---|---|---|---|
| | **Charleston, SC (CHS)** | | **Newport, NC (MHX)** | |
| **Time** | **Observed** | **CTRL** | **Observed** | **CTRL** |
| 00 UTC 14 Sept 2018 | 633.97 | 277.89 | 205.39 | 0.00 |
| 12 UTC 14 Sept 2018 | 6.82 | 0.00 | 226.42 | 416.57 |
| 00 UTC 15 Sept 2018 | 120.39 | 0.00 | 380.43 | 794.48 |
| 12 UTC 15 Sept 2018 | 3.48 | 0.01 | 694.04 | 1214.78 |
| 00 UTC 16 Sept 2018 | 102.28 | 0.90 | 762.23 | 1357.15 |
| 12 UTC 16 Sept 2018 | 107.70 | 0.00 | 570.90 | 1347.26 |
| **Average** | 162.44 | 46.47 | 473.24 | 855.04 |

**Table 4.1** CAPE values (J $kg^{-1}$) based on the observed and CTRL at 12-hourly intervals for Charleston, SC (left-of-track) and Newport, NC (right-of-track).

| CIN $\frac{J}{kg}$ | Charleston, SC (CHS 32.9, -80.03) | | Newport, NC (MHX 34.78, -76.88) | |
|---|---|---|---|---|
| Time | Observed | CTRL | Observed | CTRL |
| 00 UTC 13 Sept 2018 | 0.00 | -47.99 | -17.05 | -21.59 |
| 12 UTC 13 Sept 2018 | -0.65 | -89.04 | -9.27 | -5.72 |
| 00 UTC 14 Sept 2018 | -132.16 | -62.63 | -14.12 | 0.00 |
| 12 UTC 14 Sept 2018 | -217.82 | 0.00 | -20.37 | -2.06 |
| 00 UTC 15 Sept 2018 | 0.00 | 0.00 | -14.95 | -2.09 |
| 12 UTC 15 Sept 2018 | -5.02 | -6.42 | -21.00 | -1.73 |
| 00 UTC 16 Sept 2018 | 0.00 | -1.47 | -17.88 | -7.98 |
| 12 UTC 16 Sept 2018 | -17.68 | 0.00 | -33.36 | -5.97 |
| 00 UTC 17 Sept 2018 | -10.80 | -14.27 | -17.18 | -12.95 |
| Average | -42.68 | -24.65 | -18.35 | -6.68 |

**Table 4.2** CIN values (J $kg^{-1}$) based on the observed and CTRL at 12-hourly intervals for Charleston, SC (left-of-track) and Newport, NC (right-of-track).

MHX do not provide much insight into the background vertical wind shear. The vertical wind profile from the MHX observation (Figure 4.5c) from 950 hPa to 300 hPa gradually veers with height from the southeast to the east from 50 knots to 80 knots. Similar to the MHX observation, the CTRL (Figure 4.5d) shows a saturated, unstable atmosphere with veering winds from 950 hPa to 250 hPa and speeds between 10 knots and 40 knots. CAPE calculation for CTRL at the MHX location was 416.57 J $kg^{-1}$ (Table 4.1) and CIN was -2.06 J $kg^{-1}$ (Table 4.2). For both locations, the winds in the CTRL are weaker than observations, which indicates a weaker circulation and is consistent with the weaker central pressures. This finding is somewhat surprising given the CTRL's stronger intensity after 00 UTC 15 September (Figure 4.1c). It appears that the winds are stronger within the inner core of the simulated TC (Figure 4.1c) and

much weaker within the outer region of the TC post-landfall, shown at both sounding locations in Figure 4.5.

In order to determine if the stability left- and right-of-track is significantly different, CAPE is calculated at 12-hourly increments following the NWS observation times for CHS and MHX (Table 4.1). CAPE is then averaged for left- and right-of-track during the study period (Table 4.1). Averages for CHS (162.44 J $kg^{-1}$) and CTRL (46.47 J $kg^{-1}$) indicate that the atmosphere left-of-track is generally stable during the study period (Table 4.1). In comparison, right-of-track averages for MHX (473.24 J $kg^{-1}$) and CTRL (855.04 J $kg^{-1}$) indicate that the atmosphere is generally more unstable than left-of-track during the study period (Table 4.1). To test for statistical significance between the CAPE values for left- and right-of-track, a nonparametric Wilcoxon Signed Ranks test was performed. The Wilcoxon Signed Ranks test was selected as a viable statistical testing option since the CAPE data do not meet the normality assumption required for a Student's t-test. The Wilcoxon Signed Ranks test is used to test matched pairs of independent data for a common median value. The null hypothesis ($H_0$) tests whether the medians for left- and right-of-track CAPE are equal, while the alternative hypothesis ($H_a$) indicates the median CAPE for left- and right-of-track are different. Results with p-values of less than 0.05 indicate significance at a 95% confidence level. CAPE from observations at CHS and MHX (Table 4.1) generated a p-value of 0.062, indicating the medians for left- and right-of-track CAPE observations are not significantly different. The insignificant results for the observations could be attributed to the observation locations differing in distance from the TC track; this makes capturing the spatial variation in stability difficult.

CAPE calculated for CHS and MHX in CTRL generated a p-value of 0.014, indicating the CTRL's medians for left- and right-of-track simulated CAPE are significantly different. The

significant results for CTRL capture the variation in stability well and the positioning of the static locations likely has little impact on the test results. The results from this section suggest that stability is distributed asymmetrically around the TC center with higher instability occurring right-of-track (and downshear) and more stability occurring left-of-track (and upshear). These results do not indicate that the differences in stability are attributed to landfall, further analysis will be conducted in Chapter 5 to address the influence of landfall on stability.

### 4.4 Discussion

Further investigation into daily accumulation (Figure 4.4) shows rainfall accumulation asymmetry occurs from 14 September through 16 September when the TC tracks are close to or along the coastline; such positioning, coupled with a slow forward motion and weak vertical wind shear, isolates the land-ocean influence for the cause of the asymmetry (Chen et al., 2006). Three-hourly precipitation accumulation from 09 UTC to 12 UTC on 14 September, which covers the three hours prior to landfall, shows that the precipitation becomes more asymmetric as the TC moves over land (Figure 4.6). Throughout this same period, mid-level vertical wind shear remains weak and northwesterly (Table 4.3), which suggests that the asymmetry may have intensified as a result of landfall, similar to findings from Matyas and Cartaya (2009). The rainfall accumulation in Figure 4.6 shows a maximum (140 mm) occurring right of the TC center where the 10-m winds are strongest, similar to Chan & Liang (2003). These maxima are consistent with a principal rainband structure (Willoughby et al., 1984a). The model-derived

| Mid-level Vertical Wind Shear | Magnitude (knots) | Heading (degrees) | Summary |
|---|---|---|---|
| **14 September** | 6.6 | 112.5 | Weak, northwesterly |
| **15 September** | 7.7 | 121.25 | Weak, northwesterly |
| **16 September** | 7.4 | 104 | Weak, northwesterly |

**Table 4.3** Daily average mid-level (850-500 mb) vertical wind shear calculated using 6-hourly values from Statistical Hurricane Intensity Prediction Scheme (SHIPS).

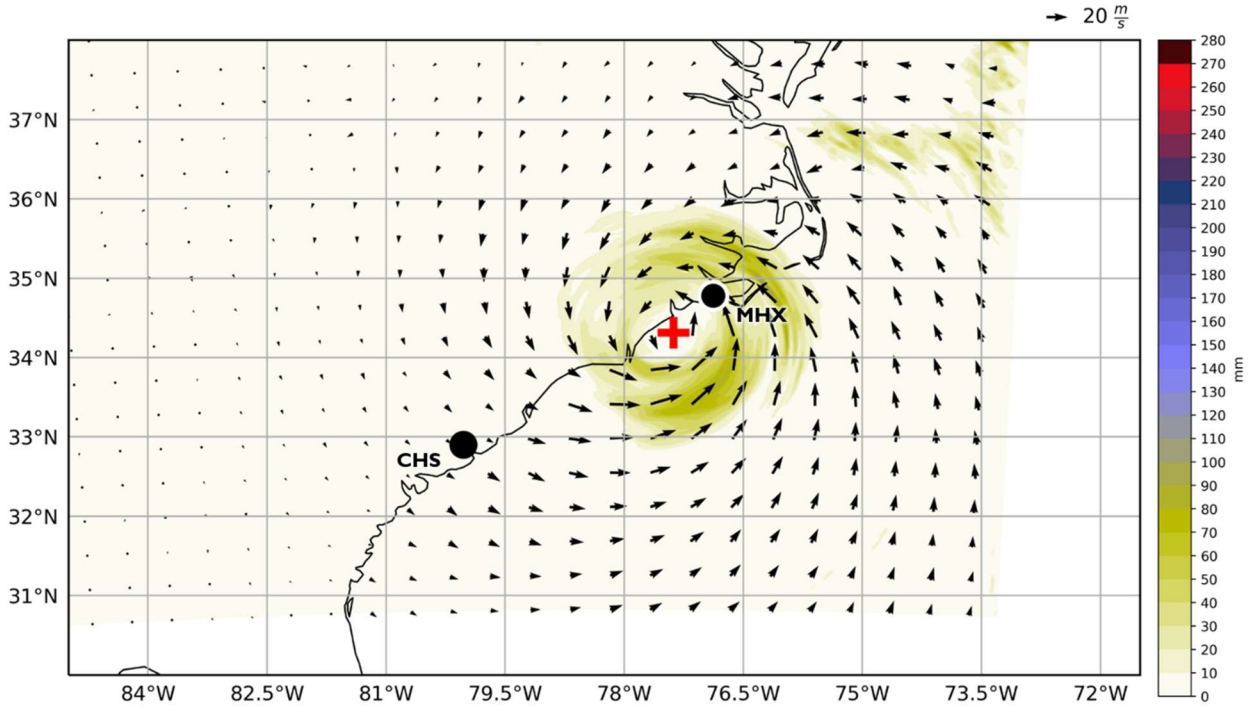


**Figure 4.6** CTRL 3-hour precipitation accumulation (mm) for 09 UTC to 12 UTC 14 September with 10-m wind speeds (m $s^{-1}$) (arrows) and TC center location ('+') at 09 UTC 14 September overlaid.

sounding at MHX (Figure 4.5d) shows an unstable atmosphere right-of-track around the time of landfall; this atmospheric profile was located approximately 85 km from the TC center and close to the location of the accumulation and wind maxima in Figure 4.6, likely near the interface of the inner core and outer core where the principal rainband is commonly found (Willoughby et al., 1984a).

The stability analysis further supports the hypothesis that the rainfall asymmetry develops in association with the spatial variation of stability. On the left-of-track side, Figure 4.5b shows a

stable atmosphere during the landfall period, coinciding with a region of no precipitation and weak 10-m winds during the 3-hour period prior to landfall (Figure 4.6). The presence of higher instability right-of-track during the landfall period coincides with the location of the maximum rainfall accumulation and stronger 10-m winds, while the stability left-of-track during landfall coincides with little precipitation accumulation and weaker 10-m winds. The lack of instability left-of-track around landfall indicates that this air mass was stable with very little buoyancy to support convection. The existence of CAPE and saturation right-of-track indicates that the atmosphere at that time is suitable for convective precipitation. This suggests that there is an asymmetrical distribution of precipitation and convection surrounding the TC in CTRL during landfall, but further analysis is required to determine whether this asymmetry is associated with landfall.

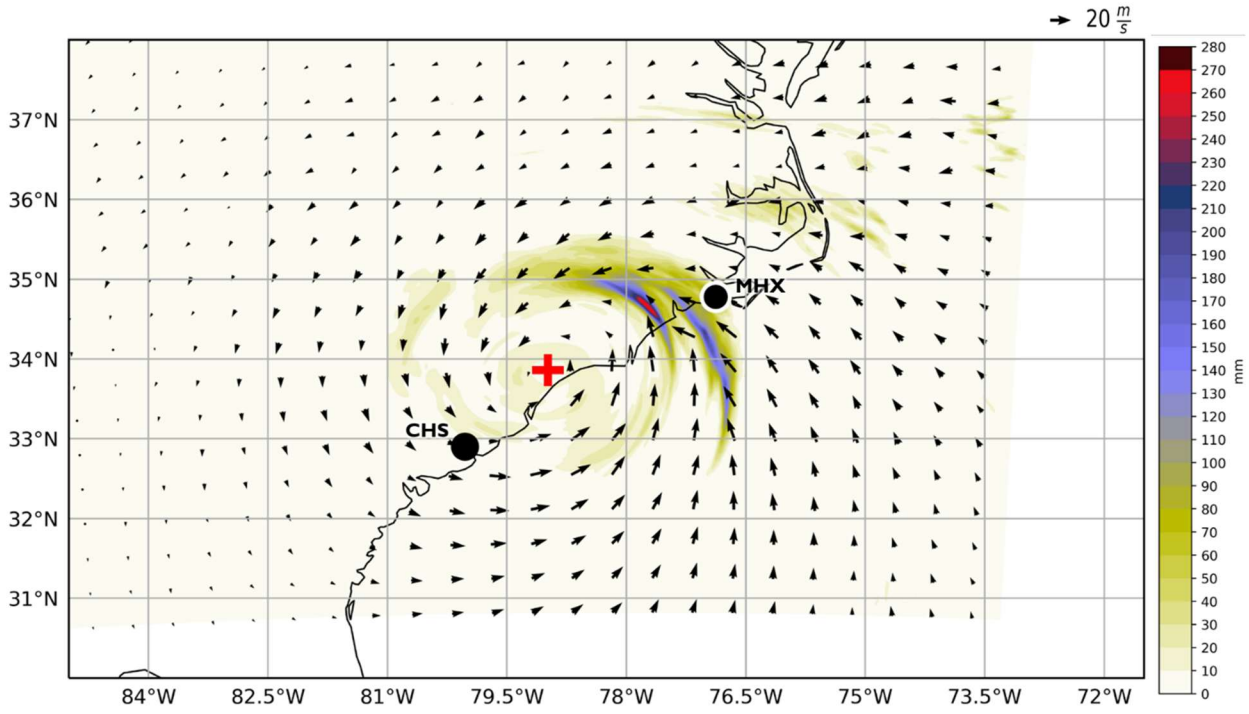

**Figure 4.7** CTRL 3-hour precipitation accumulation (mm) for 15 UTC to 18 UTC 15 September. CTRL 10-m wind speeds (m $s^{-1}$) (arrows) and center location ('+') for 15 UTC 15 September.

The relationship between rainfall accumulation asymmetries and stability is apparent during the period of slow storm motion on 15 September when the most distinct daily rainfall asymmetry occurs for both TCs (Figure 4.4c-d) and instability is greater right-of-track (Table 4.1). Between 15 UTC and 18 UTC on 15 September, the CTRL simulates the highest 3-hour rainfall maximum (267 mm) for the entire study period (Figure 4.7). Most of the precipitation occurred right of the TC center, while left of center was mostly dry. At this same time, vertical wind shear was steady at about 10 knots out of the west, possibly enhancing the asymmetry. At the start of the 3-hour period in Figure 4.7 (15 UTC 15 September), the atmospheric sounding left-of-center (denoted by CHS point on Figure 4.7) shows a stable atmosphere with low CAPE (5.28 J $kg^{-1}$) (Figure 4.8a), while the right-of-center sounding (denoted by MHX point on Figure 4.7) depicts a weakly unstable atmosphere (CAPE =914.72 J $kg^{-1}$) (Figure 4.8b). Instability right-

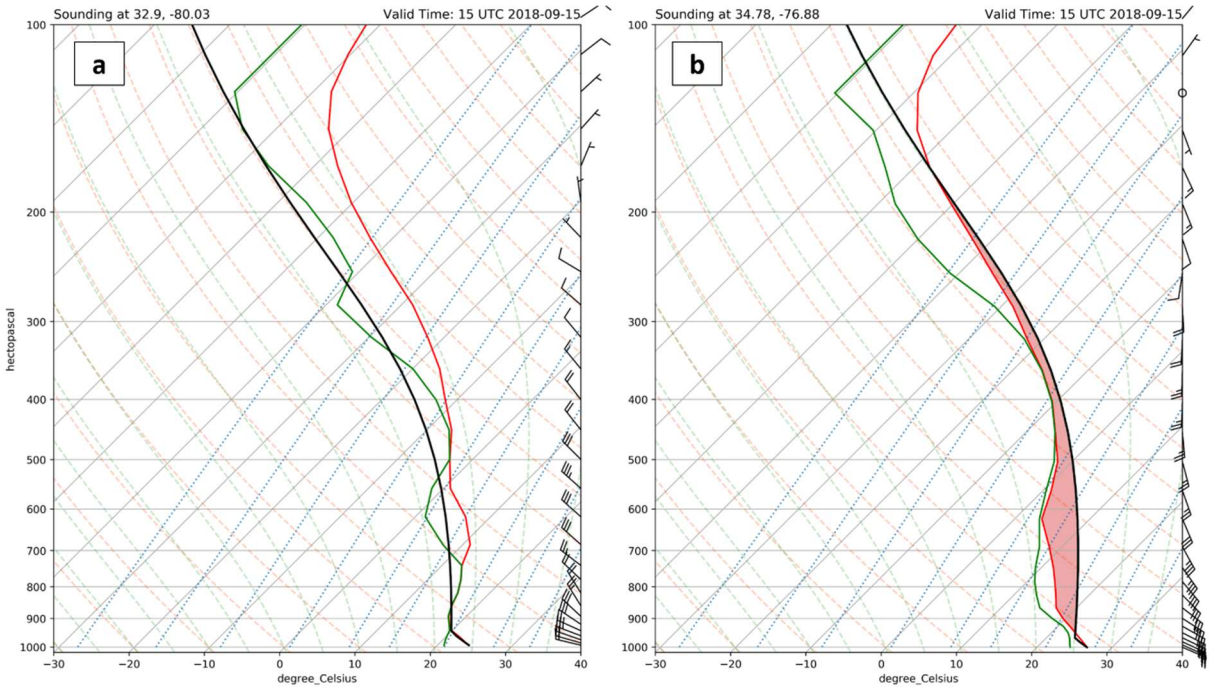

**Figure 4.8** Atmospheric soundings for CTRL at 15 UTC at the (a) CHS and (b) MHX weather stations. CAPE (J $kg^{-1}$) is shaded in red, where it exists.

of-center is co-located with the area of more intense precipitation totals and strong 10-m winds, while stability left-of-center is co-located with light precipitation totals and weak 10-m winds. The asymmetric accumulation distribution and asymmetric CAPE distribution are co-located, as higher (lower) CAPE is simulated right-of-center (left-of-center), and the higher CAPE region coincides with the CTRL and ST4 accumulation maxima (Figure 4.2). These results are consistent with the first hypothesis that asymmetries in precipitation accumulation are linked to stability surrounding a TC. However, the asymmetry cannot be completely attributed to the spatial distribution of stability due to the existence of weak vertical wind shear and the location of the principal rainband. In order to further diagnose the relationship between precipitation asymmetry and landfall, I will next conduct an experiment by altering the land surface.

## Chapter 5: Altered Land Use Simulations Results

This section compares the results from both experimental simulations with the CTRL. These comparisons address the second research question about the role of low-level moisture by altering the land surface cover to investigate differences in precipitation asymmetries during the period of time that the TCs are stationary near the coast. As noted in the methods section, the first experiment (LU11) alters the land use classes over land to be permanent wetland and the second experimental simulation (LU18) alters the land use classes over land to be wooded tundra. These land use classes were selected because they had differing values for moisture deficit (HS) but maintained the average roughness length; this should limit differences due to surface friction and isolate the influence of the surface moisture on precipitation asymmetries.

### 5.1 Track and Intensity Comparisons

The TC tracks in the experimental simulations should have little variation from CTRL because TC tracks are governed by the background steering flow (Chan, 1985), although small differences will lead to larger deviations with time (Lorenz, 1963). TC intensities have higher sensitivity to land surface characteristics. For example, TCs that move over land surfaces with high moisture and heat fluxes associated with soil conditions may reintensify (e.g., Andersen et al., 2013; Evans et al., 2011). TC tracks are analyzed in the same manner as in Chapter 4, where the TC center is the location of $MSLP_{min}$. Figure 5.1a shows the TC track and 00 UTC center locations for CTRL, LU11, and LU18 for 13 September through 17 September. A closer look at TC tracks and the 00 UTC and 12 UTC center positions from 14 September through 16 September is shown in Figure 5.1b. TC intensity measurements, $MSLP_{min}$ (mb) (Figure 5.2a) and

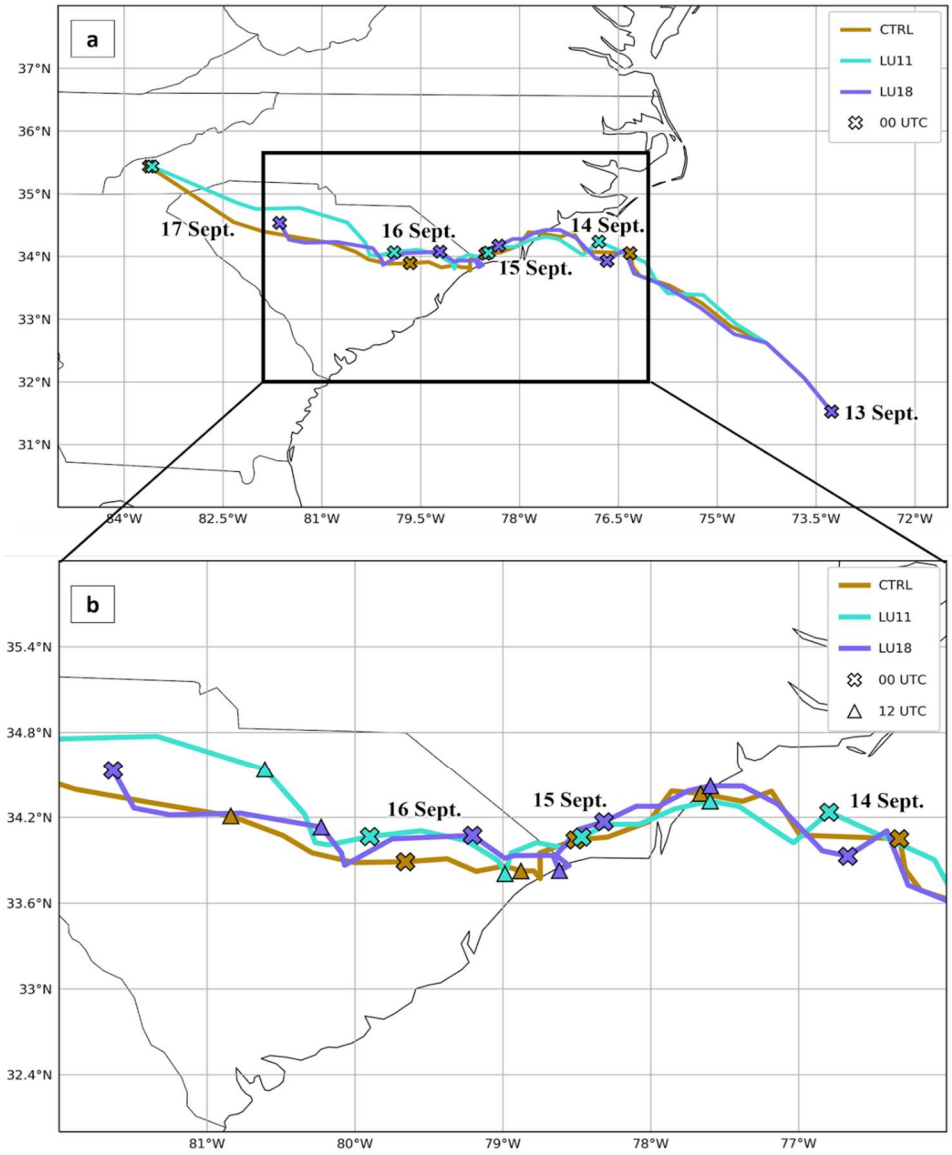


**Figure 5.1** TC center tracks for CTRL, LU11, and LU18 starting 00 UTC 13 September and ending 00 UTC 17 September (a) shows 00 UTC positions and (b) inset shows 00 UTC and 12 UTC positions.

maximum sustained 10-m winds (knots) (Figure 5.2b), are also evaluated using the same methods as Chapter 4.

Over the first 6-9 hours, we see rapid intensification (Fig 5.2) due to model spin-up, in which the lower resolution initial fields must adjust to the higher resolution model environment.

During this time, the experimental TC tracks and intensities are similar to the CTRL. Twenty-four hours into the simulation (00 UTC 14 September), LU11's TC center position has progressed farther northwest than the CTRL (Figure 5.1); during this time frame the $MSLP_{min}$ for LU11 gradually decreases, eventually reaching the lowest minimum pressure (962 mb) of any simulation for the study period just before 00 UTC 14 September (Figure 5.2a). The maximum sustained 10-m winds fluctuate between 85 and 95 knots from the end of the spin-up period through 00 UTC 14 September, indicating that the LU11 TC is at Category 2 strength during this time frame (Figure 5.2b). The simulated TC in LU11 made landfall around 13 UTC 14 September, which was approximately 2 hours after the CTRL. The LU11 track is consistently south of the CTRL track from 03 UTC 14 September through a few hours after landfall (Figure 5.1b). The $MSLP_{min}$ for LU11 gradually increases while the maximum sustained 10-m winds decrease from 03 UTC 14 September through the time of landfall, indicating that the TC weakens prior to landfall (Figure 5.2). Upon landfall, LU11 progresses slightly farther inland than CTRL until 00 UTC 15 September when TC center positions are situated around the same location (Figure 5.2). From 12 UTC 14 September to 12 UTC 15 September the distance between center positions for LU11 is small, showing the TC is nearly stationary during this time period (Figure 5.1b). Additionally, the $MSLP_{min}$ increases about 10 mb but maximum sustained 10-m winds are consistent around 60 knots, indicating little weakening of the TC intensity during that period (Figure 5.2b). The LU11 center tracks farther inland than the CTRL from 00 UTC 15 September until just before 12 UTC, after which the LU11 center moves closer to the coast, similar to the CTRL center (Figure 5.1b). LU11 slowly progresses inland in a westward direction

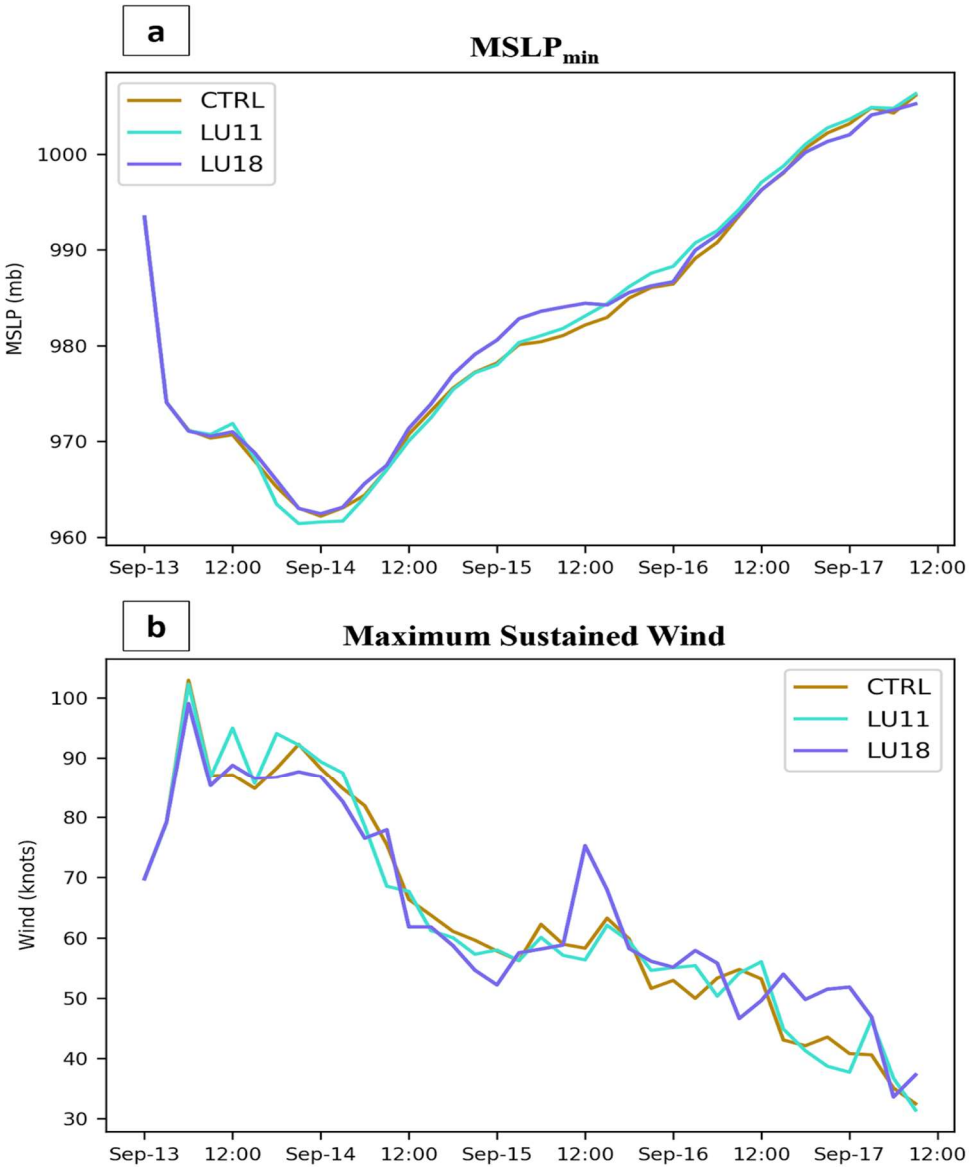


**Figure 5.2** Comparison of (a) $MSLP_{min}$ (mb) and (b) maximum sustained 10-m winds (knots) for LU11, LU18, and CTRL beginning 00 UTC 13 September and ending 00 UTC 17 September.

for the 12-hour period following 12 UTC 15 September (Figure 5.1b), during which the $MSLP_{min}$ gradually increases and maximum sustained 10-m winds slowly decrease, indicating that the TC continues to weaken (Figure 5.2). After 00 UTC 16 September, LU11 intensity weakens even further (Figure 5.2) and the center position advances northwest and is no longer situated close to

the coastline (Figure 5.1). At the end of the simulation period (00 UTC 17 September), LU11's center position is similar to CTRL's position (Figure 5.1) and the intensities are comparably weak (Figure 5.2). While minor differences exist, LU11 and CTRL have comparable tracks and intensities, as to be expected.

After the initialization period ends, LU18's track takes a course similar to, but slightly south of the CTRL through 00 UTC 14 September (Figure 5.1a). During the same period after initialization, LU18's $MSLP_{min}$ is similar to the CTRL, reaching its lowest pressure for the study period at 00 UTC 14 September (Figure 5.2a), and the maximum sustained 10-m winds maintain Category 2 strength, similar to the CTRL and LU11 (Figure 5.2b). After 00 UTC 14 September, LU18's track shifts slightly north of CTRL (and LU11) as the TC approaches the coastline (Figure 5.1b). Leading up to landfall, LU18's maximum sustained 10-m winds weakened and the $MSLP_{min}$ increased, both at a pace similar to the CTRL (and LU11) (Figure 5.2). LU18 made landfall at approximately 11 UTC 14 September, the same time as CTRL (Figure 5.1b). At landfall, LU18 had weaker maximum sustained 10-m winds of approximately 60 knots, about 5 knots less than CTRL winds, and there was a difference in $MSLP_{min}$ of less than 1 mb (Figure 5.2). In the 12-hour period after landfall, LU18 tracks slightly farther inland and slower than CTRL; the distance between the LU18 center positions for 12 UTC 14 September and 00 UTC 15 September indicate the TC is even more stationary than the CTRL TC (Figure 5.1b). Upon landfall, LU18's $MSLP_{min}$ increases more than CTRL and the maximum sustained 10-m winds weaken more than CTRL, indicating the LU18 TC intensity is weaker than both CTRL and LU11 (Figure 5.2). Between 01 UTC and 12 UTC 15 September, the maximum sustained 10-m winds for LU18 increased rapidly (Figure 5.2b), likely due to the TC center moving parallel along the coastline during that time frame (Figure 5.1b). The TC center began to move away

from the coast after 12 UTC (Figure 5.1b), and the maximum sustained 10-m winds decreased and $MSLP_{min}$ continued to increase (Figure 5.2). LU18 continued to move slower than CTRL and LU11 for the remainder of the simulation, with the 12-hourly center positions lagging behind the positions of the other simulations; this is noticeable as LU18's 00 UTC 17 September position occurred closer to the 12 UTC 16 September positions for CTRL and LU11 (Figure 5.1a). The intensity of LU18 continued to decrease with the $MSLP_{min}$ increasing similar to the CTRL and the maximum sustained 10-m winds decreasing but remaining slightly stronger than the CTRL (Figure 5.2).

Upon landfall, each of the TCs move slowly inland, tracking parallel to the coastline. The track and intensity for LU11 show slight differences compared to the CTRL; however, there are more notable differences between the LU18 and CTRL tracks and intensities. The LU11 TC is comparable to the CTRL as it progressed at a similar speed to the CTRL by remaining nearly stationary and close to the coastline from 12 UTC 14 September to 12 UTC 15 September. In comparison, the LU18 TC moved much slower than the CTRL TC upon landfall, noted by the shorter distances between 12-hourly center positions in Figure 5.1b. Additionally, the LU18 TC intensified slightly when it briefly moved parallel over the coastline around 12 UTC 15 September whereas LU11 did not show any notable signs of intensification as it was situated near the coastline. The results of the TC tracks show that all of the TCs were nearly stationary near the coast during 15 September, and the intensities of each TC were comparable. In the rest of this chapter, I will focus on the 24-hour periods before, during, and after the period of slower storm motion for the precipitation and stability analyses.

## 5.2 Precipitation Comparisons

Storm-total accumulation is used to determine if the experiments simulated asymmetrical precipitation distributions. To get a better understanding of each simulation's spatial distribution of precipitation, I will first examine the storm total precipitation for each experimental simulation by comparing it to the CTRL's accumulation in Figure 5.3a. These figures include accumulated precipitation starting at 00 UTC 13 September and ending at 09 UTC 17 September. The TC tracks and 12-hourly center positions are overlaid for context. Additionally, differences between the experiments and CTRL are calculated in Figure 5.4 by subtracting the CTRL's total accumulation from each of the experiments, with positive (negative) values indicating the experiment simulated more (less) accumulation than CTRL. These figures are used to determine if any prominent differences exist between the experiments and CTRL.

First, the differences between LU11 and CTRL are examined. Three distinct local maximums of approximately 1200 mm are present in LU11's accumulation distribution: one over the ocean left-of-track and two over land right-of-track (Figure 5.3b). LU11's storm-total maximum accumulation (1200 mm) is lower than the CTRL's maximum accumulation (1400 mm). A distinct feature of LU11's rainfall accumulation is the long swath of accumulation that expands from the ocean on the left side of the TC track to the land on the right side of the TC track (Figure 5.3b). Differences in Figure 5.4a show that LU11 simulated more accumulation inland and farther right-of-track of the TC tracks in Figure 5.1a. The difference calculation between LU11 and CTRL also shows that the LU11 simulated less accumulation in the area of the previously noted swath feature in the CTRL (Figure 5.4a). Storm-total accumulation for LU11 does show some asymmetry, but in comparison with CTRL, LU11 did not produce as strong of an asymmetrical accumulation distribution. The differences in total accumulation could

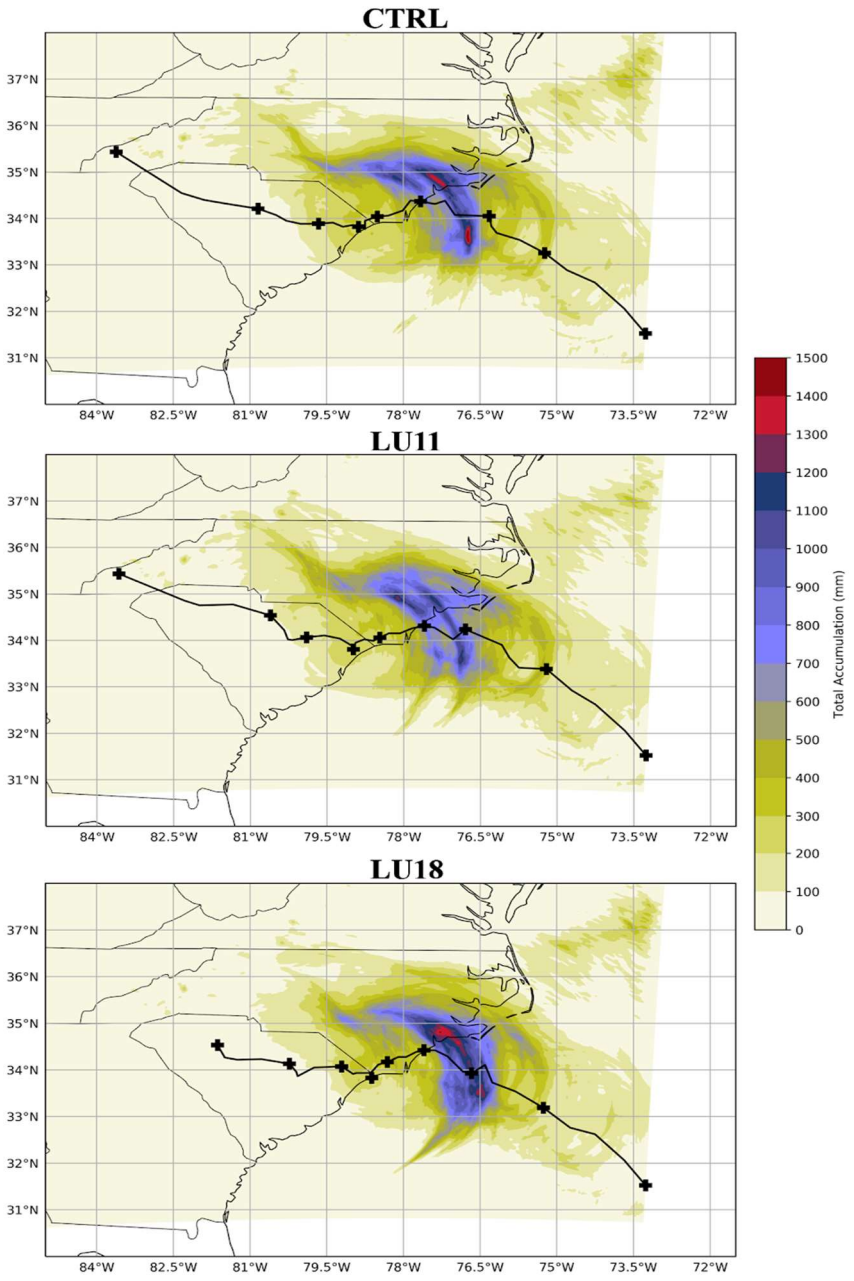


**Figure 5.3** Precipitation accumulation (mm) starting at 00 UTC 13 September 2018 and ending at 09 UTC 17 September 2018 for (a) CTRL, (b) LU11, and (c) LU18 simulations. The simulated TC tracks are overlaid with plus signs (+) for 12-hourly TC center positions starting at 00 UTC 13 September and ending at 00 UTC 17 September.

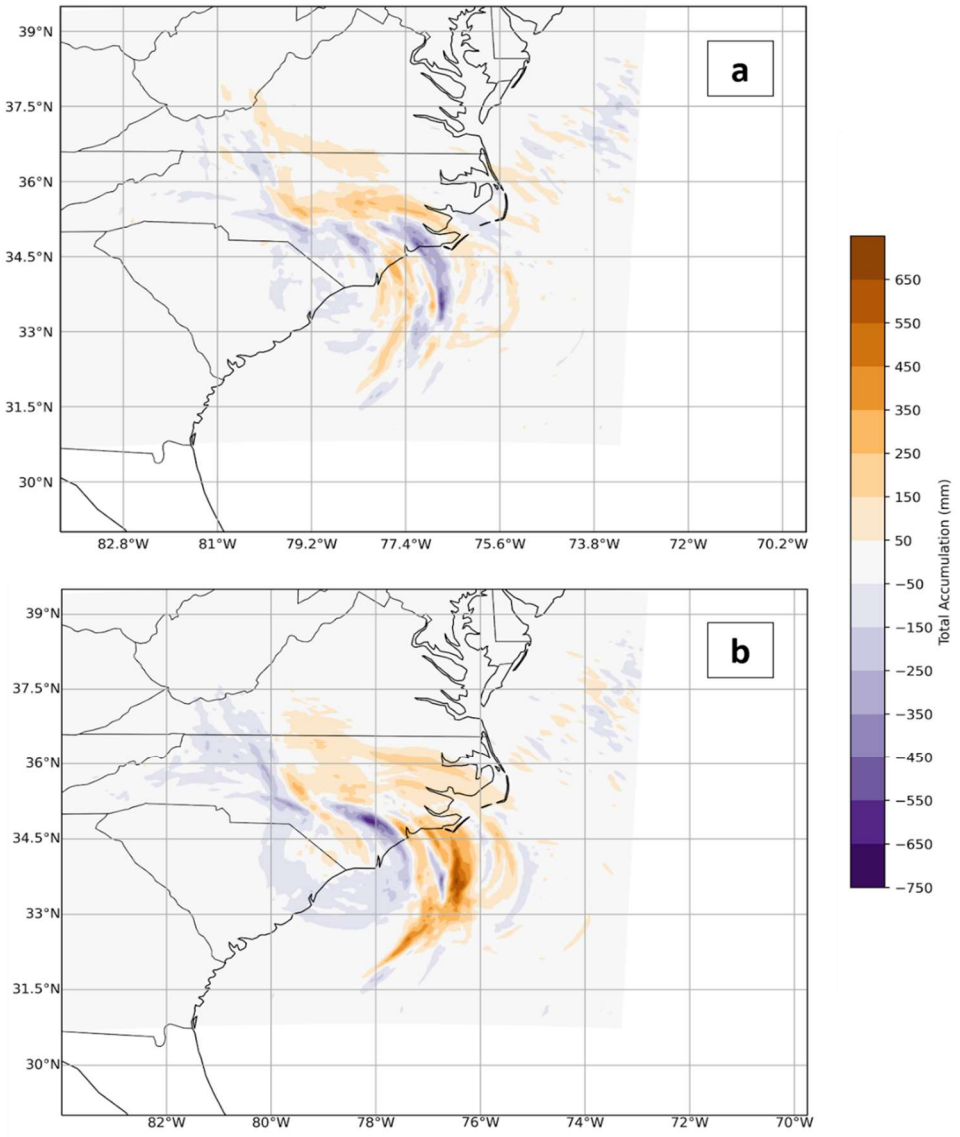


**Figure 5.4** Storm-total precipitation accumulation differences (mm) starting at 00 UTC 13 September 2018 and ending at 09 UTC 17 September 2018 for (a) LU11 minus CTRL and (b) LU18 minus CTRL.

be largely attributed to the LU11 TC moving faster than the CTRL TC, which would prevent the rainbands from training inland over the same area for an extended period of time.

Next, differences between LU18 and CTRL are examined. Storm total accumulation for LU18 shows the simulated TC generated a local accumulation maximum of approximately 1400

mm over land, right of the TC track (Figure 5.3c). LU18's local maximum (Figure 5.3c) is in a similar location as CTRL (Figure 5.3a); however, LU18 simulated a widespread area of accumulation between 1300 mm and 1400 mm surrounding the local maximum whereas the maximum occurs over a more narrow band in CTRL. The difference calculation (Figure 5.4b) shows that LU18 simulated more precipitation offshore than the CTRL. Figure 5.4b also shows LU18 simulated more accumulation farther right of the TC tracks in Figure 5.1a and simulated less accumulation in the inner core region closer to the TC tracks in Figure 5.1a.

Next, the daily accumulation is examined to determine if precipitation asymmetries are more prominent during a specific 24-hour period. The daily accumulation for LU11 (LU18) is displayed in the left (right) column of Figure 5.5 with the TC center position marked every 12 hours and the TC track overlaid. The differences in daily accumulation between LU11 (LU18) and CTRL are shown in the left (right) column of Figure 5.6. The differences are calculated by subtracting the CTRL from each experiment, meaning the positive (negative) values indicate higher (lower) accumulation for the experiments.

The results of the daily accumulation show the LU11 simulated its strongest accumulation asymmetry on 15 September when the TC was nearly stationary near the coastline. Prior to this, the daily accumulation for 14 September shows two broad areas of higher accumulation, one off-shore left-of-track and the other on-shore right-of-track, where local maxima of approximately 500 mm were simulated (Figure 5.5a). Aside from this notable feature, the differences in accumulation are relatively small, indicating that LU11's accumulation does not differ much from CTRL on 14 September (Figure 5.6a). On 15 September, LU11's simulated precipitation shows very prominent asymmetry (Figure 5.5c). A local accumulation maximum of approximately 725 mm is simulated over land, right-of-track in LU11 (Figure 5.5c); differences

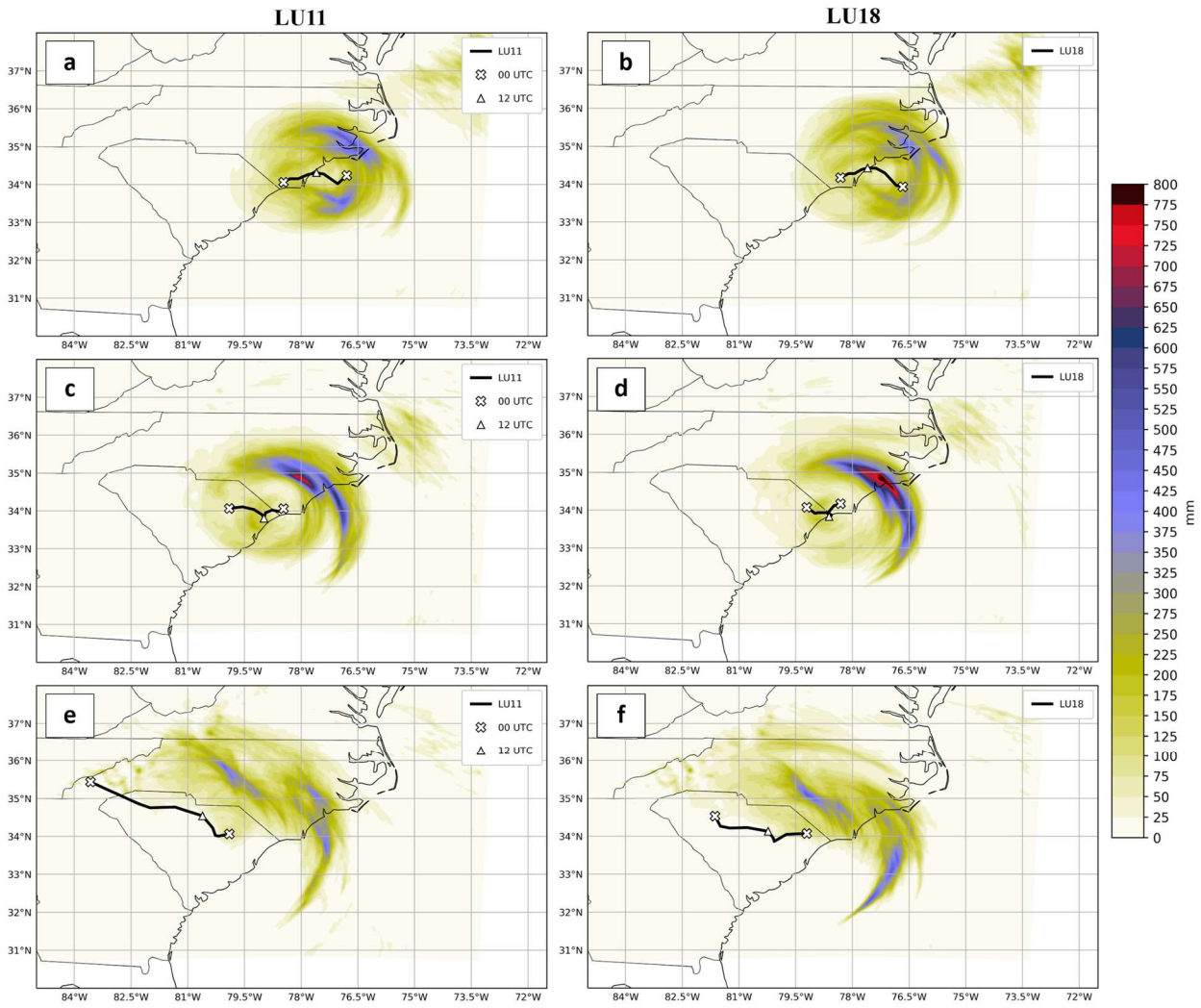


**Figure 5.5** Daily accumulated precipitation (mm) for LU11 (left) and LU18 (right) for (a-b) 14 September, (c-d) 15 September, and (e-f) 16 September. TC tracks and center positions are overlaid with a plus sign (+) for 00 UTC positions and a triangle for 12 UTC positions.

between LU11 and CTRL show LU11 simulated less accumulation in the location of the local maximum (Figure 5.6c). In comparison, the left-of-track accumulation is a widespread area of values no higher than 150 mm (Figure 5.5c), and the differences are neutral in the area of lower accumulation, meaning LU11 and CTRL simulate similar accumulations there (Figure 5.6c). The TC center positions for 15 September indicate the TC moved very little during the 24-hour

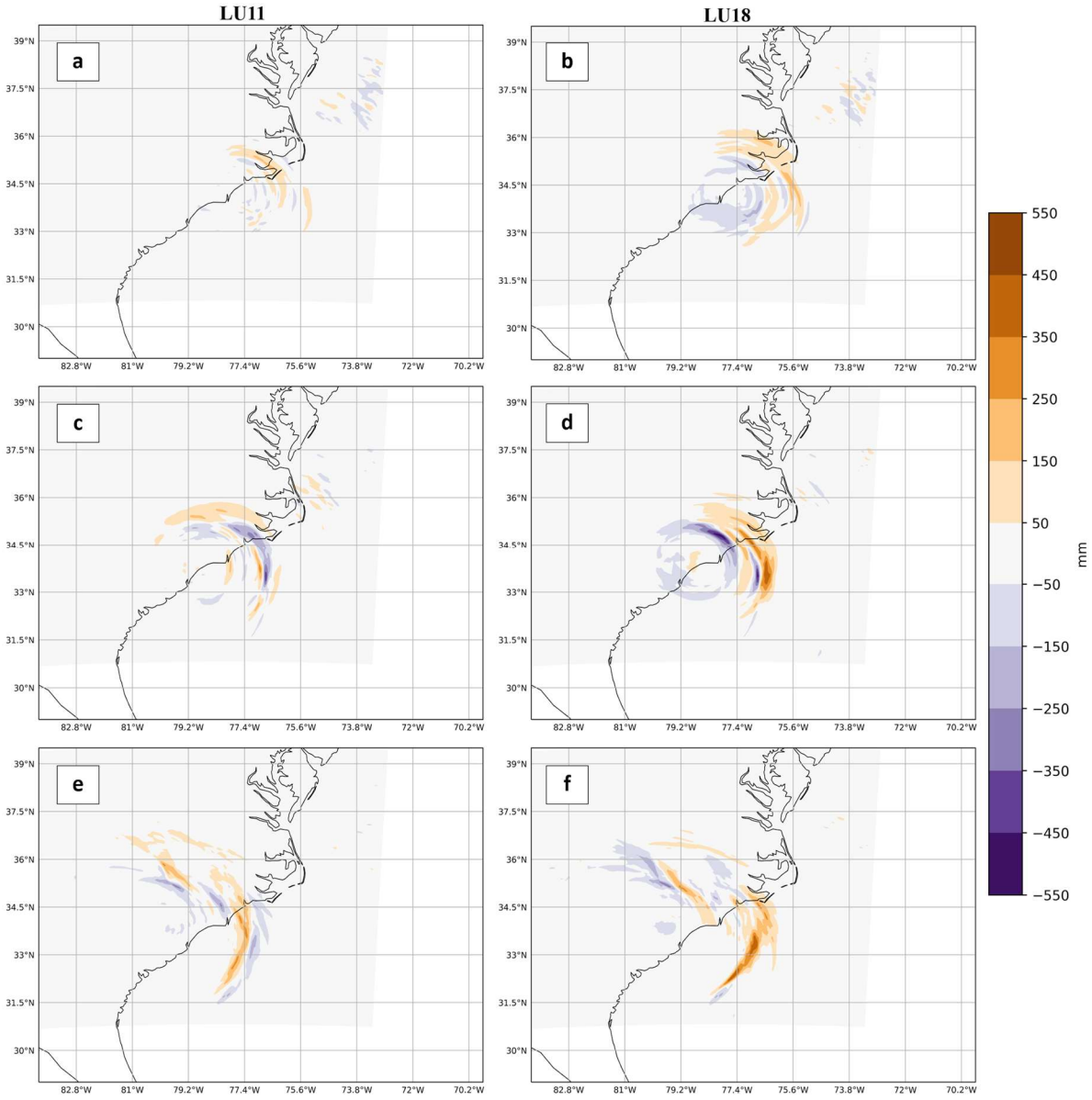


**Figure 5.6** Daily precipitation accumulation differences (mm) between (left) LU11 minus CTRL and (right) LU18 minus CTRL for (a-b) 14 September, (c-d) 15 September, and (e-f) 16 September.

period, signifying the LU11 TC is nearly stationary. The daily accumulation for 16 September shows rainfall accumulation occurred primarily right-of-track and behind the TC track, creating an asymmetrical distribution during the 24-hour period (Figure 5.5e). Differences show LU11

simulated about 250 mm more accumulation over the ocean (Figure 5.6e). LU11's center positions for 16 September indicate the TC is no longer nearly stationary near the coast and accumulation asymmetry may be attributed to multiple factors including storm motion and vertical wind shear.

Prominent accumulation asymmetry was simulated in LU18 on 15 September when accumulation was minimal close to the TC center and higher farther away from the center. Before the time period with greatest asymmetry, daily accumulation displayed weaker asymmetry. Daily accumulation for LU18 on 14 September shows some asymmetry since there are higher values (approximately 400 mm) of simulated accumulation right of the TC track over land while left-of-track over land the simulated accumulation is much lower (approximately 150 mm) (Figure 5.5b). The differences show that LU18 simulated more accumulation farther from the TC track and less accumulation closer to the TC track (Figure 5.6b). On 15 September LU18 simulated distinct accumulation asymmetry where a local maximum of approximately 800 mm is right-of-track within a long swath of precipitation that is situated over ocean and land (Figure 5.5d). LU18 simulated more accumulation than CTRL in the area of the distinct swath in Figure 5.5d with a maximum difference of approximately 450 mm (Figure 5.6d). Situated close to the maximum difference is a small area of less accumulation for LU18 (Figure 5.6d). The negative difference is likely from a difference in rainband location for LU18. The positions of TC center in Figure 5.5d show that LU18 moved very little during that 24-hour period of the simulation, indicating the TC is nearly stationary near the coast throughout 15 September. The accumulation distribution for 16 September shows the accumulation is simulated far right-of-track as well as close to the track (Figure 5.5f). One area with a local accumulation maximum (approximately 400 mm) is simulated over land right-of-track and a second maximum (approximately 500 mm)

is simulated over ocean (Figure 5.5f). Differences from the CTRL indicate LU18 simulated more accumulation over the ocean (Figure 5.6f). These results show that LU18's daily accumulation was asymmetrical during the three 24-hour periods analyzed.

### 5.3 Atmospheric Stability Comparisons

As mentioned in Chapter 4, atmospheric stability varies surrounding a TC (Chan & Liang, 2003), and results from the CTRL suggest that there is more instability right-of-track than left-of-track for a near-perpendicular landfall. This atmospheric stability section will investigate the differences in stability between the experimental simulations and CTRL. I start by first comparing the simulated values for CAPE to the right and left of LU11 and LU18 TC tracks. Four static locations were chosen to extract values of CAPE: two left-of-track and two right-of-track (Figure 5.7). The four locations were chosen for their distance from the TC center, as they

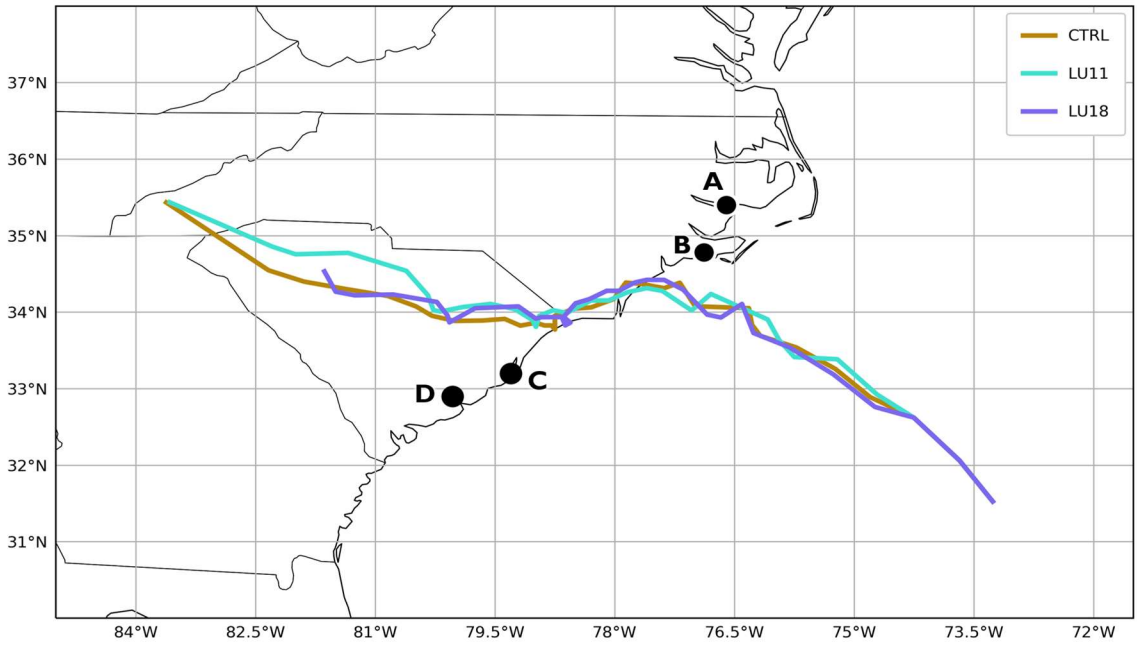


**Figure 5.7** Static locations A, B, C, and D used for calculating point values of CAPE. Simulated TC tracks are overlaid for spatial reference.

remain mostly out of the influence of the inner core during the study period, and proximity to the coastline, which is important to capture the stability of air masses that move on-shore right-of-track and off-shore left-of-track. CAPE values were calculated every 3 hours (00 UTC 14 September through 21 UTC 16 September) for each location to get a better understanding of how CAPE evolved at the static locations prior to, during, and after landfall. Daily means and medians of CAPE were determined for each simulation using the 3-hourly calculations of CAPE for the static locations (Table 5.1).

| | CTRL | | LU11 | | LU18 | |
|---|---|---|---|---|---|---|
| | **Right-of-track** | **Left-of-track** | **Right-of-track** | **Left-of-track** | **Right-of-track** | **Left-of-track** |
| **14 September** | 433.77 | 58.21 | 510.44 | 57.55 | 444.29 | 43.60 |
| **15 September** | 870.87 | 4.40 | 847.63 | 17.69 | 535.82 | 6.60 |
| **16 September** | 1081.57 | 191.40 | 1188.44 | 240.47 | 578.25 | 53.48 |
| **Mean** | 795.40 | 84.67 | 857.84 | 105.23 | 519.45 | 34.56 |
| **Median** | 771.46 | 2.44 | 810.39 | 6.59 | 443.09 | 4.07 |

**Table 5.1** Daily averages of simulated CAPE for CTRL, LU11, and LU18 at the two right-of-track and two left-of-track locations shown in Figure 5.7. Means and medians shown in the bottom two rows were calculated from 3-hourly CAPE values from 00 UTC 14 September through 00 UTC 17 September.

Averages of CAPE indicate the stability of the atmosphere varies from left- to right-of-track for both experimental simulations (Table 5.1). Additionally, there are some differences among the CAPE medians for the three simulations. LU11's average for CAPE right-of-track (857.84 J/kg) is greater than CTRL (795.40 J/kg) (Table 5.1). The median CAPE for LU11 (810.39 J/kg) was also slightly greater than CTRL (771.46 J/kg) (Table 5.1). This is interesting to note because LU11 produced lower local accumulation maximums than CTRL. LU18's total average for CAPE right-of-track (519.45 J/kg) is much lower than CTRL average (Table 5.1).

The median CAPE for LU18 (443.09 J/kg) is also much lower than CTRL median (Table 5.1). This result is interesting because the precipitation accumulation for LU18 was more prominent than CTRL and LU11 and high local maxima were simulated in LU18. Left-of-track means and medians of CAPE for LU11 (105.23 J/kg and 6.59 J/kg respectively) and LU18 (34.56 J/kg and 4.07 J/kg respectively) were much lower than right-of-track averages, similar to CTRL (84.67 J/kg and 2.44 J/kg).

The results show differences between the simulated CAPE for right- and left-of-track for all simulations, leading to the need to test for statistical significance. Similar to the stability section in Chapter 5, a Wilcoxon Signed Ranks test was conducted to test if the left- and right-of-track CAPE median values are significantly different for each simulation. Right-of-track and left-of-track CAPE values during each time step were paired to perform the test. Table 5.2 displays the results of the Wilcoxon Signed Ranks test. These p-values (Table 5.2) indicate that for each simulation, the medians for left- and right-of-track CAPE are significantly different, consistent with the CTRL results in Chapter 4.

| | **CTRL** | **LU11** | **LU18** |
|---|---|---|---|
| **p-value** | <0.0001 | <0.0001 | <0.0001 |

**Table 5.2** Results of the Wilcoxon Signed Ranks test for right- and left-of track differences in CAPE for the CTRL, LU11, and LU18 simulations.

### 5.4 Discussion

The experimental simulations were conducted to investigate differences in TC precipitation distributions during a period of slow storm motion by altering the land surface to be more moist (LU11) or drier (LU18). By altering the land surface, symmetry in the spatial

distributions of precipitation and stability should be distinguishable. TC tracks and intensities suggest that the movement and strength of the TCs in each experiment were not sensitive to the altered land cover; this is to be expected as TCs are steered by the large-scale winds. A positive outcome of this is that each of the simulated TCs became stationary upon landfall, allowing for differences in precipitation and stability to be examined without the need of ruling out other physical influences. The differences in storm-total accumulation between the experiments and CTRL indicate that the spatial distributions of precipitation accumulation differ somewhat, even though an asymmetry is evident in both LU11 and LU18. Compared to CTRL and LU18, the LU11 TC generated a lower local storm-total maximum over land and ocean, which suggests that the TC may not have simulated very robust convection on the right side of the storm, even though the CAPE right-of-track average for LU11 was higher than LU18 and CTRL. However, LU18's storm total accumulation had a high local maxima right-of-track similar to CTRL, suggesting that LU18 precipitation was more asymmetrical than LU11.

The results of LU11 and LU18 show the simulated TCs produced asymmetric rainfall accumulation September 14 through September 16, the same period that the TCs were nearly stationary near the coastline. Accumulations for 14 September show minor differences between the experiments and CTRL, which is assumed to be due to the TCs beginning to interact with the land surface during that period. The most prominent accumulation asymmetry is simulated on 15 September when the TCs are nearly stationary close to the coast. LU18's strong asymmetry during the 15 September accumulation period suggests that as the TC was situated near the coast, the rainbands training inland were convective in nature, producing heavy precipitation as the air mass moved further inland before stabilizing inland. Similarly, LU11 simulated an asymmetrical

precipitation distribution during the same time period, suggesting that there are other physical factors that are influencing the generation of precipitation asymmetries.

The change in land surface is hypothesized to impact the stability surrounding the TCs due to the availability of moisture in the surface boundary layer. A moister land surface should promote symmetrical distributions in stability and precipitation while a drier land surface should encourage asymmetrical distributions to form. Following my hypothesis, 6-hour average differences in 950 mb relative humidity (Figure 5.8) ending at 00 UTC 15 September indicate LU11 simulated more moisture over land than CTRL and LU18 simulated less moisture over land than the CTRL. The differences in 950 mb relative humidity confirm that altering the land surface to be more moist or dry led to similar changes in moisture in the atmosphere overlying that land surface. However, the influence of the moisture availability at the surface does not

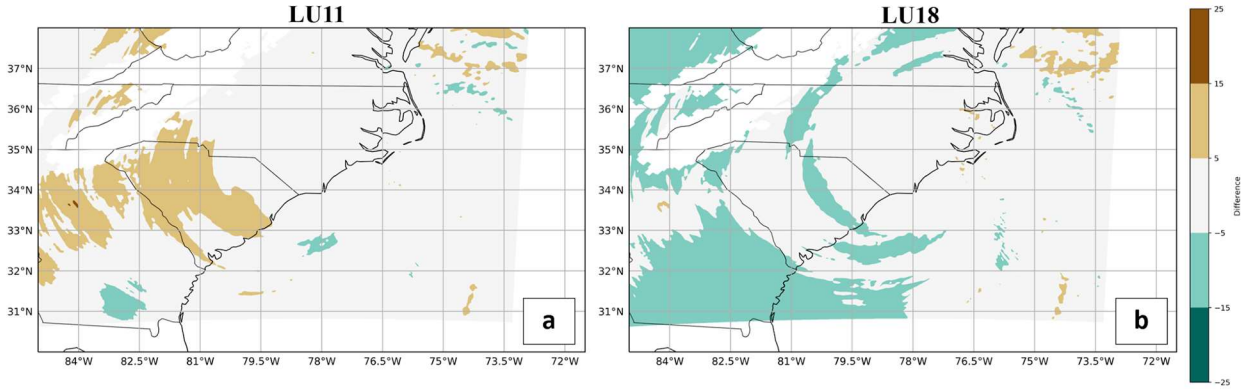


**Figure 5.8** Average 950 mb relative humidity from 18 UTC 14 September through 00 UTC 15 September for (a) LU11 minus CTRL and (b) LU18 minus CTRL. Positive (negative) values indicate the experiment simulated higher (lower) 950 mb relative humidity than CTRL.

appear to impact vertical levels above 950 mb (not shown). There is also minimal impact of the low-level moisture on the spatial distribution of CAPE. Figure 5.9 shows a 3-hour average of

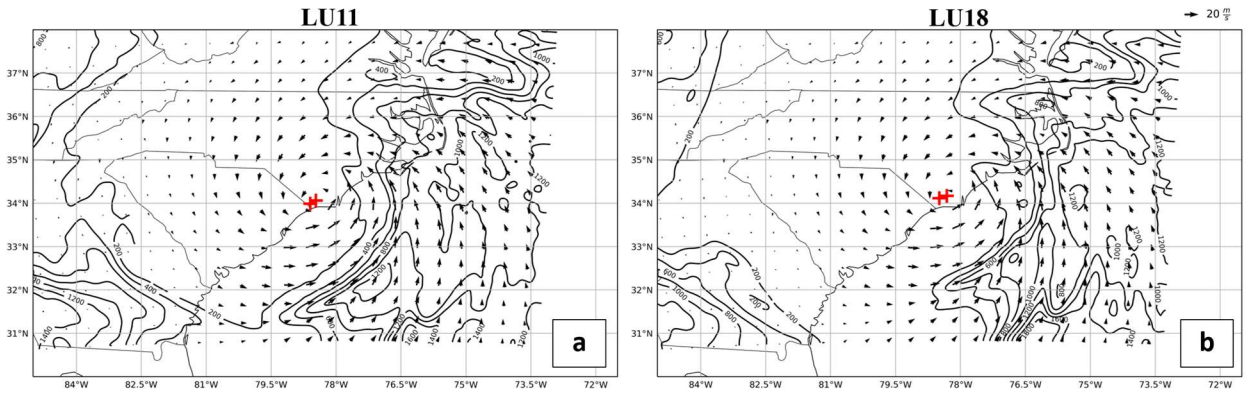


**Figure 5.9** 3-hour averaged CAPE (contours) and 10-meter winds (m $s^{-1}$) (arrows) ending at 03 UTC 15 September for (a) LU11 and (b) LU18. Plus signs (+) denote the TC center positions at 00 UTC and 03 UTC on 15 September.

CAPE and 10-m winds (m $s^{-1}$) ending at 03 UTC 15 September for both experimental simulations. Overall, visual inspection indicates that the CAPE has little variation between experiments in the region where CAPE is greatest over ocean and to the right of the TC center over land (Figure 5.9). The most notable difference is the existence of CAPE just off-shore at the southern extent of the domain for LU11 (Figure 5.9a) where there is zero CAPE for LU18 (Figure 5.9b). It appears the CAPE is influenced immediately off-shore left of the TC center positions, but the overall distribution is affected very little by the altered land surface. According to the hypothesis, a moister surface boundary layer would enhance instability off-shore left of the TC center while a drier surface boundary layer would promote stability off-shore left of TC center. Results in Figure 5.9 indicate that these changes in instability (as measured by CAPE) were much smaller than hypothesized. Furthermore, the accumulation during the same 3-hour period as Figure 5.9 is inconsistent with the hypothesis as both LU11 and LU18 simulated asymmetrical precipitation distributions (Figure 5.10). The lack of variability between

distributions for precipitation (Figure 5.10) and CAPE (Figure 5.9) further suggests that other physical factors are contributing to the observed precipitation asymmetries.

## Chapter 6: Conclusion and Future Work

The purpose of this study was to understand TC precipitation asymmetries that occur during the landfall period when Hurricane Florence (2018) was nearly stationary parallel to the coastline. Asymmetries in convective precipitation are often caused by various influences of landfall, including surface friction, dry air intrusion, topography, and vertical wind shear. Outer rainbands contribute to stronger asymmetry in precipitation during the landfall period. The outer rainbands often form in areas of higher instability, which produces robust convection and often heavier precipitation that trains inland on the right side of the TC during landfall. Since the outer rainbands are sensitive to the surrounding environment, this study focuses on the relationship between stability surrounding Hurricane Florence and associated precipitation asymmetries.

Influences of precipitation asymmetries were explored further by analyzing the influence of land cover, and subsequently low-level moisture, on the stability surrounding the TCs. The period of near-stationary motion during Hurricane Florence's landfall allowed for a more thorough investigation of the influence of different land cover surfaces on precipitation asymmetries. The precipitation asymmetries in post-landfall stationary TCs were hypothesized to be linked to differences in stability in the outer environment of the TC. To address this hypothesis, a control simulation of Hurricane Florence was generated and then modified by altering the land surface cover for land. This study investigated whether low-level moisture associated with the land surface impacted the atmospheric stability surrounding the TC. Two experiments were conducted, one with lower moisture availability (LU18) and one with higher moisture availability (LU11), while surface roughness remained nearly constant. Based on the hypothesis, LU11 would lead to more symmetry in precipitation during landfall and LU18 would enhance precipitation asymmetry during the landfall period.

Before analyzing the experimental simulations, the control simulation was examined to better understand the relationship between precipitation asymmetries and stability surrounding Hurricane Florence. The tracks of the observed and CTRL TCs were very similar, each making landfall around the same time and location and experiencing a period of slow storm motion paralleling the coast post-landfall. The period of slow storm motion was the focal point of this study, in hopes of isolating the land-sea interaction influence on the stability in the outer rainband region surrounding the TCs. Comparisons of observed and CTRL storm total accumulation show that both TCs displayed asymmetrical precipitation distributions as most of the precipitation was right-of-track.

Strong precipitation asymmetry during the period of slow storm motion on 15 September was primarily attributed to the location of the principal rainband and weak mid-level vertical wind shear, similar to findings by Matyas & Cartaya (2009) that suggest slow storm motion and weak shear can cause precipitation to be concentrated right-of-track. The largest difference between the observed and CTRL precipitation distributions was the location and intensity of rainbands. Stage IV estimates showed more precipitation fell closer to the TC track while most of the CTRL precipitation was simulated northeast of the TC track. The spatial differences in accumulation are likely attributed to numerous influences including slight differences in the post-landfall TC tracks, intensities, location of rainbands, and the presence of weak vertical wind shear (Matyas & Cartaya, 2009). Distribution of stability surrounding the TCs was similar, where the right-of-track static locations simulated higher CAPE than the left-of-track locations. However, the Wilcoxon Signed Ranks test results indicated the left- and right-of-track CAPE values were not significantly different for observations while CTRL results suggest there was a significant difference. The insignificant results for CAPE observations may have been due to the

NWS observation locations differing in distance from the storm track; if the observations were taken from similar distances to the TC track, the results may have yielded a significant difference. These findings suggest that (1) the precipitation distributions and stability surrounding the TCs are asymmetric for the real and observed TCs, (2) more precipitation occurred right-of-track and (3) there was higher instability right-of-track. However, other physical factors, such as the presence of weak vertical wind shear, could have also contributed to the asymmetries. Further analysis of the influences of the precipitation asymmetries during the landfall period was necessary to draw a stronger conclusion.

To address the second research question, two experimental simulations (LU11 and LU18) were created to isolate the influence of land surface moisture on the precipitation asymmetry during the period of slow storm motion. When comparing the differences in storm total and daily precipitation accumulations with the CTRL, both experimental simulations produced asymmetrical precipitation distributions. The moist land surface simulation (LU11) produced lower accumulation maximums for the storm-total and daily accumulation periods while the drier land surface simulation (LU18) generated stronger accumulation asymmetries for the storm-total and daily accumulation periods. For both LU11 and LU18, CAPE at the static locations right-of-track was significantly different from CAPE at the left-of-track locations during the time period the TCs were stationary near the coast. It was noted that the 950 mb relative humidity displayed an increase (LU11) or decrease (LU18) in low-level moisture over land, and three hours later, a noticeable increase (LU11) or decrease (LU18) in CAPE is simulated immediately off-shore left-of-track for each experiment. These results suggest that altering the land surface affects moisture from the surface to about 950 mb which impacts stability immediately off-shore on the left side of the TC circulation. However, the alteration of low-level moisture over land was found to not

have a significant impact on the precipitation asymmetries in both experiments. The results of LU18 follow the hypothesis that a drier land surface would cause a landfalling TC to have well-defined asymmetry in the precipitation distribution. However, the results of LU11 do not follow the hypothesis that a moister land surface would cause a landfalling TC's precipitation distribution to be more symmetrical because LU11 also simulates an asymmetrical precipitation distribution. Other physical factors may have a stronger impact on precipitation during the landfall period. One possibility is the influence of topography since the topographic features remained constant in all simulations. As mentioned in Chapter 2, topography is known to enhance precipitation asymmetry during the landfall period (e.g., Matyas, 2007). Another possible factor aiding in the generation of the precipitation asymmetries is the advection of warm, moist air from the tropical region south of the domain (e.g., Matyas, 2017). Similar conclusions were found in a study of Hurricane Harvey (Galarneau & Zeng, 2020). This moisture transport process remains untouched in the CTRL and LU11 and LU18 experiments, potentially allowing enough moisture to fuel convection in the simulated TCs and ultimately preventing the altered low-level moisture to affect the entire TC structure. Vertical wind shear may also contribute to the development of the convective asymmetries, as CAPE is generally highest downshear and downshear left (Molinari & Vollaro, 2010). Overall, these results suggest that there is not an apparent impact of low-level moisture on precipitation asymmetries during landfall.

The results of this study were inconclusive because the low-level moisture from the land surface had no influence on large-scale CAPE, leaving precipitation asymmetries unexplained. Further work needs to be conducted to fully diagnose the relationship between stability and precipitation asymmetries during the landfall period. Future studies should investigate additional

land surface types; specifically, it would be interesting to alter the land surface to be categorized as ocean to determine if asymmetries exist in a completely moist environment with negligible surface friction. Additionally, future studies should consider removing topography to create a completely flat domain to determine if the asymmetries are due to topographical forcing. An alternate approach to the stability analysis should also be considered in future work. This could be addressed by calculating moving spatial averages of CAPE and precipitation accumulation (centered on the TC) left- and right-of-track for each TC prior to, during, and after landfall. Such an analysis would help draw a stronger conclusion as to how the asymmetries evolve as the TCs approach and interact with the land surface. Furthermore, CAPE alone does not provide a complete understanding of atmospheric stability surrounding the landfalling TCs. Additional moving spatial averages for all relevant mesoscale stability indices, e.g., the KI, which factors in the importance of low-level moisture, should be included to better diagnose relationships between stability and precipitation asymmetries during TC landfall. Finally, an ensemble of experimental simulations should be conducted to account for initial condition and/or model uncertainty. The results of these additional analyses would form a stronger conclusion on the relationship between stability and asymmetrical precipitation distributions during the TC landfall period.

## References


Andersen, T. K., Radcliffe, D. E., & Shepherd, J. M. (2013). Quantifying surface energy fluxes in the vicinity of inland-tracking tropical cyclones. *Journal of Applied Meteorology and Climatology*, *52*(12), 2797–2808. https://doi.org/10.1175/JAMC-D-13-035.1

Atallah, E., Bosart, L. F., & Aiyyer, A. R. (2007). Precipitation Distribution Associated with Landfalling Tropical Cyclones over the Eastern United States. *Monthly Weather Review*, *135*(6), 2185–2206. https://doi.org/10.1175/MWR3382.1

Blake, E. S., & Zelinsky, D. A. (2017). *HURRICANE HARVEY*.

Bracken, W. E., & Bosart, L. F. (2000). The role of synoptic-scale flow during tropical cyclogenesis over the North Atlantic Ocean. *Monthly Weather Review*, *128*(2), 353–376. https://doi.org/10.1175/1520-0493(2000)128<0353:TROSSF>2.0.CO;2

Bui, H. H., Smith, R. K., Montgomery, M. T., & Peng, J. (2009). Balanced and unbalanced aspects of tropical cyclone intensification. *Quarterly Journal of the Royal Meteorological Society*, *135*(644), 1715–1731. https://doi.org/10.1002/qj.502

Chan, J. C.L. (1985). Identification of the steering flow for tropical cyclone motion from objectively analyzed wind fields. *Monthly Weather Review*, *113*(1), 106–116. https://doi.org/10.1175/1520-0493(1985)113<0106:IOTSFF>2.0.CO;2

Chan, Johnny C. L., Liu, K. S., Ching, S., & Lai, E. (2004). Asymmetric Distribution of Convection Associated with Tropical Cyclones Making Landfall along the South China Coast. *Monthly Weather Review*, *132*, 2410–2420. https://doi.org/https://doi.org/10.1175/1520-0493(2004)132<2410:ADOCAW>2.0.CO;2

Chan, Johnny C.L., & Liang, X. (2003). Convective asymmetries associated with tropical cyclone landfall. Part I: f-plane simulations. *Journal of the Atmospheric Sciences*, *60*(13), 1560–1576. https://doi.org/10.1175/1520-0469(2003)60<1560:CAAWTC>2.0.CO;2

Chan, K. T. F., Chan, J. C. L., & Wong, W. K. (2019). Rainfall asymmetries of landfalling tropical cyclones along the South China coast. *Meteorological Applications*, *26*(2), 213–220. https://doi.org/10.1002/met.1754

Chen, F., & Dudhia, J. (2001). Coupling an Advanced Land Surface–Hydrology Model with the Penn State–NCAR MM5 Modeling System. Part I: Model Implementation and Sensitivity. *Monthly Weather Review*, *129*, 569–585. https://doi.org/10.1175/1520-0493(2001)129<0569:CAALSH>2.0.CO;2

Chen, S. S., Knaff, J. A., & Marks, F. D. (2006). Effects of vertical wind shear and storm motion on tropical cyclone rainfall asymmetries deduced from TRMM. *Monthly Weather Review*, *134*(11), 3190–3208. https://doi.org/10.1175/MWR3245.1

Davis, C., Wang, W., Chen, S. S., Chen, Y., Corbosiero, K., DeMaria, M., Dudhia, J., Holland, G., Klemp, J., Michalakes, J., Reeves, H., Rotunno, R., Synder, C., & Xiao, Q. (2008). Prediction of landfalling hurricanes with the advanced hurricane WRF model. *Monthly Weather Review*, *136*(6), 1990–2005. https://doi.org/10.1175/2007MWR2085.1

Demaria, M., & Kaplan, J. (1994). A statistical hurricane intensity prediction scheme (SHIPS) for the Atlantic Basin. *Weather & Forecasting*, *9*(2), 209–220. https://doi.org/10.1175/1520-0434(1994)009<0209:ASHIPS>2.0.CO;2

Didlake, A. C., & Houze, R. A. (2009). Convective-scale downdrafts in the principal rainband of hurricane Katrina (2005). *Monthly Weather Review*, *137*(10), 3269–3293. https://doi.org/10.1175/2009MWR2827.1

Dunion, J. P. (2011). Rewriting the climatology of the tropical North atlantic and Caribbean Sea

atmosphere. *Journal of Climate*, *24*(3), 893–908. https://doi.org/10.1175/2010JCLI3496.1
Evans, C., Schumacher, R. S., & Galarneau, T. J. (2011). Sensitivity in the overland reintensification of Tropical Cyclone Erin (2007) to near-surface soil moisture characteristics. *Monthly Weather Review*, *139*(12), 3848–3870. https://doi.org/10.1175/2011MWR3593.1
Fudeyasu, H., & Wang, Y. (2011). Balanced Contribution to the Intensification of a Tropical Cyclone Simulated in TCM4: Outer-Core Spinup Process. *J. Atmos. Sci.*, *68*(3), 430–449. https://doi.org/10.1175/2010JAS3523.1
Galarneau, T. J., & Zeng, X. (2020). The hurricane harvey (2017) Texas rainstorm: Synoptic analysis and sensitivity to soil moisture. *Monthly Weather Review*, *148*(6), 2479–2502. https://doi.org/10.1175/MWR-D-19-0308.1
Gray, W. M. (1968). Global View of the Origin of Tropical Disturbances and Storms. *Monthly Weather Review*, *96*(10), 669–700. https://doi.org/10.1175/1520-0493(1968)096<0669:gvotoo>2.0.co;2
Guo, Q., & Matyas, C. J. (2016). Comparing the spatial extent of Atlantic basin tropical cyclone wind and rain fields prior to land interaction. *Physical Geography*, *37*(1), 5–25. https://doi.org/10.1080/02723646.2016.1142929
Halverson, J. B., Simpson, J., Heymsfield, G., Pierce, H., Hock, T., & Ritchie, L. (2006). Warm core structure of Hurricane Erin diagnosed from high altitude dropsondes during CAMEX-4. *Journal of the Atmospheric Sciences*, *63*(1), 309–324. https://doi.org/10.1175/JAS3596.1
Houze Jr., R. A. (2010). Clouds in tropical cyclones. *Monthly Weather Review*, *138*(2), 293–344. https://doi.org/10.1175/2009MWR2989.1
Jiang, H., Ramirez, E. M., & Cecil, D. J. (2013). Convective and Rainfall Properties of Tropical Cyclone Inner Cores and Rainbands from 11 Years of TRMM Data. *Monthly Weather Review*. https://doi.org/10.1175/MWR-D-11-00360.1
Junker, N. W., Schneider, R. S., & Fauver, S. L. (1999). A Study of Heavy Rainfall Events during the Great Midwest Flood of 1993. *Weather and Forecasting*, *14*(5), 701–712. https://doi.org/10.1175/1520-0434(1999)014<0701:ASOHRE>2.0.CO;2
Kellner, O., Niyogi, D., Lei, M., & Kumar, A. (2012). The role of anomalous soil moisture on the inland reintensification of Tropical Storm Erin (2007). *Natural Hazards*, *63*(3), 1573–1600. https://doi.org/10.1007/s11069-011-9966-6
Kimball, S. K. (2006). A Modeling Study of Hurricane Landfall in a Dry Environment. *Monthly Weather Review*, *134*(7), 1901–1918. https://doi.org/10.1175/MWR3155.1
Kimball, S. K. (2008). Structure and Evolution of Rainfall in Numerically Simulated Landfalling Hurricanes. *Monthly Weather Review*, *136*(10), 3822–3847. https://doi.org/10.1175/2008MWR2304.1
Kishtawal, C. M., Niyogi, D., Kumar, A., Bozeman, M. L., & Kellner, O. (2012). Sensitivity of inland decay of North Atlantic tropical cyclones to soil parameters. *Natural Hazards*, *63*(3), 1527–1542. https://doi.org/10.1007/s11069-011-0015-2
Klotzbach, P. J., Bowen, S. G., Pielke, R., & Bell, M. (2018). Continental U.S. Hurricane Landfall Frequency and Associated Damage: Observations and Future Risks. *Bulletin of the American Meteorological Society*, *99*(7), 1359–1376. https://doi.org/10.1175/BAMS-D-17-0184.1
Leroux, M.-D., Wood, K., Elsberry, R. L., Cayanan, E. O., Hendricks, E., Kucas, M., Otto, P., Rogers, R., Sampson, B., & Yu, Z. (2018). Recent Advances in Research and Forecasting of Tropical Cyclone Track, Intensity, and Structure at Landfall. *Tropical Cyclone Research*

*and Review*, *7*(2), 85–105. https://doi.org/10.6057/2018TCRR02.02
Li, Q., & Wang, Y. (2012). A Comparison of Inner and Outer Spiral Rainbands in a Numerically Simulated Tropical Cyclone. *Monthly Weather Review2*. https://doi.org/10.1175/MWR-D-11-00237.1
Lorenz, E. N. (1963). Deterministic Nonperiodic Flow. *Journal of the Atmospheric Sciences*, *20*(2), 130–141. https://doi.org/10.1175/1520-0469(1963)020<0130:dnf>2.0.co;2
Maddox, R. A., Chappell, C. F., & Hoxit, L. R. (1979). Synoptic and meso-scale aspects of flash flood events. *Bulletin, American Meteorological Society*, *60*(2), 115–123. https://doi.org/10.1175/1520-0477-60.2.115
Markowski, P., & Richardson, Y. (2010). Mesoscale Meteorology in Midlatitudes. In *Mesoscale Meteorology in Midlatitudes*. Wiley Blackwell. https://doi.org/10.1002/9780470682104
Matyas, C. (2007). Quantifying the shapes of U.S. landfalling tropical cyclone rain shields. *Professional Geographer*, *59*(2), 158–172. https://doi.org/10.1111/j.1467-9272.2007.00604.x
Matyas, C. (2017). Comparing the Spatial Patterns of Rainfall and Atmospheric Moisture among Tropical Cyclones Having a Track Similar to Hurricane Irene (2011). *Atmosphere*, *8*(12), 165. https://doi.org/10.3390/atmos8090165
Matyas, C. J. (2010). A geospatial analysis of convective rainfall regions within tropical cyclones after landfall. *International Journal of Applied Geospatial Research*, *1*(2), 71–91. https://doi.org/10.4018/jagr.2010020905
Matyas, C. J., & Cartaya, M. (2009). Comparing the Rainfall Patterns Produced by Hurricanes Frances (2004) and Jeanne (2004) over Florida. *Southeastern Geographer*, *49*(2), 132–156. https://doi.org/10.1353/sgo.0.0046
Mitchell, K. (2005). *The community Noah land-surface model (LSM)*.
Molinari, J., Romps, D. M., Vollaro, D., & Nguyen, L. (2012). CAPE in Tropical Cyclones. *Journal of the Atmospheric Sciences*, *69*(8), 2452–2463. https://doi.org/10.1175/JAS-D-11-0254.1
Molinari, J., & Vollaro, D. (2010). Distribution of Helicity, CAPE, and Shear in Tropical Cyclones. *Journal of the Atmospheric Sciences*, *67*(1), 274–284. https://doi.org/10.1175/2009JAS3090.1
Montgomery, M. T., & Kallenbach, R. J. (1997). A theory for vortex rossby-waves and its application to spiral bands and intensity changes in hurricanes. *Quarterly Journal of the Royal Meteorological Society*, *123*(538), 435–465. https://doi.org/10.1002/qj.49712353810
Paul, S., Ghebreyesus, D., & Sharif, H. (2019). Brief Communication: Analysis of the Fatalities and Socio-Economic Impacts Caused by Hurricane Florence. *Geosciences*, *9*(2), 58. https://doi.org/10.3390/geosciences9020058
Powell, M. D. (1987). Changes in the low-level kinematic and thermodynamic structure of Hurricane Alicia ( 1983) at Landfall. *Monthly Weather Review*, *115*(1), 75–99. https://doi.org/10.1175/1520-0493(1987)115<0075:CITLLK>2.0.CO;2
Powell, M. D. (1990). Boundary layer structure and dynamics in outer hurricane rainbands. Part I: mesoscale rainfall and kinematic structure. *Monthly Weather Review*, *118*(4), 891–917. https://doi.org/10.1175/1520-0493(1990)118<0891:BLSADI>2.0.CO;2
Ryzhkov, A., & Zrnic, D. S. (1995). Precipitation and Attenuation Measurements at a 10-cm Wavelength. *Journal of Applied Meteorology and Climatology*, *34*(10). https://doi.org/10.1175/1520-0450(1995)034%3C2120:PAAMAA%3E2.0.CO;2
Schnetzler, A. E. (2008). *Analysis of twenty-five years of heavy rainfall events in the Texas Hill*

*Country* [University of Missouri--Columbia]. https://doi.org/10.32469/10355/5792
Shea, D. J., & Gray, W. M. (1973). The Hurricane's Inner Core Region. I. Symmetric and Asymmetric Structure. *Journal of the Atmospheric Sciences*, *30*(8), 1544–1564. https://doi.org/10.1175/1520-0469(1973)030<1544:thicri>2.0.co;2
Skamarock, W. C., Klemp, J. B., Dudhia, J., Gill, D. O., Barker, D. M., Duda, M. G., Huang, X.-Y., Wang, W., & Powers, J. G. (2008). *A Description of the Advanced Research WRF Version 3*.
Srivastava, P. K., Han, D., Rico-Ramirez, M. A., Al-Shrafany, D., & Islam, T. (2013). Data Fusion Techniques for Improving Soil Moisture Deficit Using SMOS Satellite and WRF-NOAH Land Surface Model. *Water Resources Management*, *27*(15), 5069–5087. https://doi.org/10.1007/s11269-013-0452-7
Stern, D. P., & Nolan, D. S. (2012). On the Height of the Warm Core in Tropical Cyclones. *Journal of the Atmospheric Sciences*, *69*(5), 1657–1680. https://doi.org/10.1175/JAS-D-11-010.1
Stewart, S. R. (2001). *Tropical Cyclone Report: Tropical Cyclone Allison*.
Stewart, S. R., & Berg, R. (2019). *Hurricane Florence*.
Stull, R. B. (2012). *An introduction to boundary layer meteorology* (Volume 13). Springer Science & Business Media.
Sugg, A. L., & Pelissier, J. M. (1968). The Hurricane Season of 1967. *Monthly Weather Review*, *96*(4), 242–250. https://doi.org/10.1175/1520-0493(1968)096<0242:thso>2.0.co;2
Thomas, D. S. G. (2016). *The dictionary of physical geography* (D. S. G. Thomas (ed.); Fourth Edi). John Wiley & Sons Ltd.
Vahmani, P., & Hogue, T. S. (2014). Incorporating an Urban Irrigation Module into the Noah Land Surface Model Coupled with an Urban Canopy Model. *Journal of Hydrometeorology*, *15*(4), 1440–1456. https://doi.org/10.1175/jhm-d-13-0121.1
Villarini, G., Smith, J. A., Baeck, M. L., Marchok, T., & Vecchi, G. A. (2011). Characterization of rainfall distribution and flooding associated with U.S. landfalling tropical cyclones: Analyses of Hurricanes Frances, Ivan, and Jeanne (2004). *Journal of Geophysical Research Atmospheres*, *116*(23). https://doi.org/10.1029/2011JD016175
Weatherford, C. L., & Gray, W. M. (1988a). Typhoon structure as revealed by aircraft reconnaissance. Part I: data analysis and climatology. *Monthly Weather Review*, *116*(5), 1032–1043. https://doi.org/10.1175/1520-0493(1988)116<1032:TSARBA>2.0.CO;2
Weatherford, C. L., & Gray, W. M. (1988b). Typhoon structure as revealed by aircraft reconnaissance. Part II: structural variability. *Monthly Weather Review*, *116*(5), 1044–1056. https://doi.org/10.1175/1520-0493(1988)116<1044:TSARBA>2.0.CO;2
Willoughby, H. E. (1988). Willoughby1988_AusMetMag.pdf. *Australian Meteorological Magazine*, *36*(3), 183–191.
Willoughby, H. E. (1990). Gradient Balance in Tropical Cyclones. *Journal of the Atmospheric Sciences*, *47*, 265–274. https://doi.org/10.1175/1520-0469(1990)047<0265:GBITC>2.0.CO;2
Willoughby, H. E., Marks, F. D., & Feinberg, R. H. (1984a). Stationary and moving convective bands in hurricanes. *Journal of the Atmospheric Sciences*, *41*(22), 3189–3211. https://doi.org/10.1175/1520-0469(1984)041<3189:SAMCBI>2.0.CO;2
Willoughby, H. E., Marks, F. D., & Feinberg, R. H. (1984b). Stationary and moving convective bands in hurricanes. *Journal of the Atmospheric Sciences*, *41*(22), 3189–3211. https://doi.org/10.1175/1520-0469(1984)041<3189:SAMCBI>2.0.CO;2

Xu, W., Jiang, H., & Kang, X. (2014). Rainfall asymmetries of tropical cyclones prior to, during, and after making landfall in South China and Southeast United States. *Atmospheric Research*, *139*, 18–26. https://doi.org/10.1016/j.atmosres.2013.12.015

Yang, L., Smith, J., Liu, M., & Baeck, M. L. (2019). Extreme rainfall from Hurricane Harvey (2017): Empirical intercomparisons of WRF simulations and polarimetric radar fields. *Atmospheric Research*. https://doi.org/10.1016/j.atmosres.2019.03.004

Zhou, Y., Matyas, C., Li, H., & Tang, J. (2018). Conditions associated with rain field size for tropical cyclones landfalling over the Eastern United States. *Atmospheric Research*, *214*, 375–385. https://doi.org/10.1016/j.atmosres.2018.08.019

Zipser, E. J. (1977). Mesoscale and Convective–Scale Downdrafts as Distinct Components of Squall-Line Structure. *Monthly Weather Review*, *105*(12), 1568–1589. https://doi.org/10.1175/1520-0493(1977)105<1568:macdad>2.0.co;2